Gravity Wave Perturbations of Minor Constituents: A Parcel Advection Methodology

STEPHEN D. ECKERMANN*

Computational Physics, Inc., Fairfax, Virginia

DOROTHY E. GIBSON-WILDE

Colorado Research Associates, Boulder, Colorado

JULIO T. BACMEISTER

E. O. Hulburt Center for Space Research, Naval Research Laboratory, Washington, D.C.

(Manuscript received 20 May 1997, in final form 10 February 1998)

ABSTRACT

Existing analytical models of wave-induced minor constituent fluctuations result from linearized perturbation expansions of a rate equation governing either number density or mixing ratio, whereas many numerical models now use isentropic parcel advection methods to simulate these effects. Exact relationships between the two approaches are not currently clear for gravity waves. Here, the parcel advection method is formalized and applied to derive analytical formulas for the response of vertical constituent profiles of arbitrary shape to adiabatic gravity wave displacements. These relations are compared to corresponding formulas from standard linearized perturbation analyses. Both methods accurately model perturbations produced by nondissipating hydrostatic gravity waves within idealized vertical tracer profiles. Both methods can also model wave-induced perturbations of minor constituents with shorter chemical lifetimes. This is demonstrated by using the parcel method to reproduce previous results for wave-induced fluctuations in upper-stratospheric ozone. The parcel-based approach yields more accurate models of nondissipating hydrostatic gravity wave effects on tracer distibutions with sharp spatial gradients. The authors demonstrate this by using the method to model wave-induced modulations of sporadic sodium layers in the mesosphere and of ozone laminae in the lower stratosphere. Conversely, the parcel method does not accurately model tracer density perturbations produced by nonhydrostatic waves, or situations in which the photochemical response of the constituent leads to significant diabatic feedback on the perturbing wave.

1. Introduction

High-resolution observations of minor (trace) constituents in the middle and upper atmosphere often reveal small-scale perturbations superimposed upon the mean background distribution. Such features can be produced by any number and combination of dynamical, radiative, and chemical processes. For trace constituents with long lifetimes, however, dynamics must be predominately responsible for any observed variability of that constituent's local number density over shorter timescales.

One important source of such variability is waves. For instance, vertical soundings at middle and high latitudes often reveal large enhancements or depletions of lower-stratospheric ozone (a tracer at these heights) confined to narrow ($\sim$1–2 km) vertical layers (e.g., Reid and Vaughan 1991; Bird et al. 1997). These structures, known assortedly as filaments or laminae, result from complex synoptic-scale flow patterns produced by breaking planetary Rossby waves, which yield air parcels at different stratospheric levels with vastly different histories and, hence, constituent densities (e.g., Newman and Schoeberl 1995; Orsolini et al. 1997).

Oblique oscillatory displacements of air parcels from their equilibrium positions produce accompanying density and temperature changes that can also perturb constituent profiles. Oscillations due to various types of planetary waves have been found to induce related perturbations in ozone (e.g., Newman and Randel 1988;

* Current affiliation: E. O. Hulburt Center for Space Research, Naval Research Laboratory, Washington, D.C.

Corresponding author address: Dr. Stephen D. Eckermann, Computational Physics, Inc., Suite 600, 2750 Prosperity Avenue, Fairfax, VA 22031.
E-mail: eckerman@cpi.com.

Prata 1990; Hess 1990; Randel and Gille 1991; Randel 1993; Stanford and Ziemke 1993; Wirth 1993; Ziemke and Stanford 1994; Engelen 1996) and other trace constituents (e.g., Randel 1990; Salby et al. 1990; Limpasuvan and Leovy 1995). On smaller scales, internal gravity waves can also give rise to fluctuations in constituent profiles (e.g., Reber et al. 1975; Gardner and Shelton 1985; Hedin and Mayr 1987; Sugiyama 1988; Hoegy et al. 1990; Wilson et al. 1991; Alexander and Pfister 1995; Langford et al. 1996; Bian et al. 1996; Bacmeister et al. 1997).

In fact, since observational data on middle and upper atmosphere constituents are often better and more abundant than wind and temperature data, analyses of fluctuations in long-term measurements of constituent densities have been used to infer climatologies of both planetary waves and gravity waves (e.g., Randel and Gille 1991; Senft and Gardner 1991; Randel 1993; Ziemke and Stanford 1994; Collins et al. 1996). However, since the response of constituents to waves is usually not straightforward, wave properties must be inferred from such observations by using a wave–tracer interaction model to convert the measured constituent response into a wave-related quantity. Such conversion methods have been derived to date by applying standard linearized perturbation methods of gravity wave theory to rate equations governing constituent densities or mixing ratios. Such derivations yield analytical formulas for translating conventional gravity wave oscillations into a corresponding response in the constituent profile (e.g., Dudis and Reber 1976; Chiu and Ching 1978; Gardner and Shelton 1985). Such relations can then be used to convert observed constituent fluctuations into wave-related quantities (e.g., Gardner and Voelz 1985; Randel 1990; Senft and Gardner 1991).

Recently, detailed numerical models have provided new insights into the way minor constituents respond to planetary wave and gravity wave advection (e.g., Fritts et al. 1993, 1997; Waugh et al. 1994; Roble and Shepherd 1997). Rich complex structures in minor species distributions are simulated, which often resemble observations (e.g., Fritts et al. 1993, 1997) but are not predicted by standard formulas that convert between observed tracer variability and a plane monochromatic wave. Due to their complexity, however, these models cannot as yet be used for operational extraction of wave properties from observed constituent fluctuations in the atmosphere. On the other hand, simplified versions of these models, which retained the minimum terms needed to simulate the basic effects, might lead to improved analytical models of wave-induced perturbations of minor constituent profiles.

We investigate this possibility here by considering one class of these numerical models, the so-called trajectory or parcel advection models. They have proved successful in simulating finescale tracer structures in the stratosphere, often using wind and temperature data with much coarser spatiotemporal resolution (e.g., Newman and Schoeberl 1995; Orsolini et al. 1997). The models work well because their assumptions of adiabatic motion and long chemical lifetimes are well satisified for many constituents in the lower stratosphere, where diabatic heating and turbulent diffusivities are both small. However, constituents with shorter chemical lifetimes can also be simulated by these models if a suitable parcel-based chemistry scheme is used (e.g., Lutman et al. 1997). Even in the troposphere, where diffusion and diabatic heating can be large, parcel advection models that parameterize these effects have also proved to be useful tools (e.g., Kao et al. 1995; Rind and Lerner 1996).

Given that parcel advection models often perform well even after many days of integration, the same models should also perform well if the synoptic-scale advection patterns were supplemented with wave-induced advection effects since their timescales (periods) are of the order of days for planetary waves and less than a day for gravity waves. Furthermore, since many gravity waves and planetary waves propagate conservatively through the stratosphere, an assumption of adiabatic wave-induced advection should also be well satisfied. Indeed, limited tests of gravity wave effects in such models have used this sort of approach (Pierce et al. 1994; Jensen and Thomas 1994; Carslaw et al. 1998).

Thus, we formalize the basic physical concepts underpinning parcel advection models in section 2, assess the utility of the method in gravity wave studies, then apply it in section 3 to derive analytical responses of tracers to wave-induced displacements. We compare our results throughout with corresponding results using the traditional approach of expanding state parameters into the sum of a mean and perturbation term, then isolating and linearizing the perturbation terms in the governing equations. Results of these analyses and intercomparisons are summarized in section 4.

2. Air parcel approach

This approach is based on the classic meteorological problem of vertically displacing a small dry parcel of air from its equilibrium height, where it is ''well mixed'' and in thermal equilibrium with the surrounding atmosphere. We assume that the displacement is small and that the parcel responds adiabatically while always maintaining a pressure equal to that of the surrounding atmosphere, following standard conventions (see, e.g., section 2.5.1 of Wallace and Hobbs 1977; section 9.1 of Iribarne and Godson 1981).

a. Conserved quantities in the parcel

1) TRACER MIXING RATIO

We consider a constituent of number density n within an air parcel of total number density n_M. For a trace constituent $n/n_M \ll 1$, any changes in n produce neg-

ligible changes in n_M, whereupon the following continuity equations apply:

$$\frac{dn_M}{dt} + n_M \nabla \cdot \mathbf{U} = 0 \tag{1a}$$

$$\frac{dn}{dt} + n \nabla \cdot \mathbf{U} = R, \tag{1b}$$

where $\mathbf{U}$ is the local velocity vector, $d/dt = \partial/\partial t + \mathbf{U} \cdot \nabla$ is a time derivative in the Lagrangian (parcel following) frame ($\partial/\partial t$ is the ground-based Eulerian time derivative), and R is the net production/loss rate for the trace constituent's number density n. Eliminating $\nabla \cdot \mathbf{U}$ between (1a) and (1b) yields (Lindzen and Goody 1965)

$$\frac{d}{dt}\left(\frac{n}{n_M}\right) = \frac{dq}{dt} = \frac{R}{n_M}, \tag{2}$$

where q is the mixing ratio of the trace constituent.

For passive trace constituents, $R \approx 0$, whereupon (2) yields

$$\frac{dq}{dt} = 0, \tag{3a}$$

or

$$q = \frac{n}{n_M} = \text{const} \tag{3b}$$

within the parcel. Thus, we get the well-known result that passive trace constituents are also tracers since the movement of a region of unique constituent mixing ratio traces the Lagrangian motion of air parcels.

2) Potential temperature

Air parcels advected by an inviscid adiabatic flow also conserve potential temperature Θ so that

$$\frac{d\Theta}{dt} = 0. \tag{4}$$

For a horizontally homogeneous atmosphere, the background potential temperature Θ is given by Poisson's relation

$$\overline{\Theta}(z) = \overline{T}(z)\left(\frac{\overline{p}(z_0)}{\overline{p}(z)}\right)^{(\gamma-1)/\gamma} = T(z, z_0), \tag{5}$$

where z is height, γ is the ratio of specific heats, $\overline{T}(z)$ is the background temperature, and $\overline{p}(z)$ is the background pressure (e.g., Turner 1973). From (5), $\overline{\Theta}(z)$ is also equal to the temperature $T(z, z_0)$ that an air parcel attains on being transported adiabatically a distance δz from its rest height z to a new height $z_0 = z + \delta z$.

3) Potential density

We can also work in terms of potential density, $D(z)$, which is defined for a horizontally homogeneous background atmosphere as

$$\overline{D}(z) = \overline{\rho}(z)\left(\frac{\overline{p}(z_0)}{\overline{p}(z)}\right)^{1/\gamma} = \rho(z, z_0) \tag{6}$$

(e.g. Turner 1973), where $\overline{\rho}(z) = M\overline{n}_M(z)$ is the background total air density at height z, $\overline{n}_M(z)$ is the background total number density, and M is the mean mass of an air molecule, assumed constant (no diffusive separation). From (6), $\overline{D}(z)$ also equals the density $\rho(z, z_0)$ that an air parcel attains on being transported adiabatically from a pressure, $\overline{p}(z)$ and density $\overline{\rho}(z)$, at its rest height z to a reference pressure $\overline{p}(z_0)$ at the displaced height $z_0 = z + \delta z$. It then follows (e.g., Wallace and Hobbs 1977) that

$$\frac{dD}{dt} = 0 \tag{7}$$

for parcels on an inviscid adiabatic flow, and thus the potential density of any parcel within such a flow is also conserved.

4) Potential tracer density

Analogously, we can also define a potential density, Δ, for a given tracer. If the constituent in question behaves as a tracer at all heights and has negligible horizontal gradients in its distribution, then, as in (6), we can define a background potential tracer density profile given by

$$\overline{\Delta}(z) = M_{tc}\overline{\nu}(z) = M_{tc}\overline{n}(z)\left(\frac{\overline{p}(z_0)}{\overline{p}(z)}\right)^{1/\gamma} = M_{tc}n(z, z_0), \tag{8}$$

where M_{tc} is the molecular mass of the trace constituent and $\overline{\nu}(z)$ is the background potential number density of the tracer. From (8), we see that $\overline{\Delta}(z)$ also equals the mass density of tracer $M_{tc}n(z, z_0)$ that an air parcel contains after being transported adiabatically from a pressure $\overline{p}(z)$ and tracer density $M_{tc}\overline{n}(z)$ at its rest height z to a reference pressure $\overline{p}(z_0)$ at the new height $z_0 = z + \delta z$. It then follows that

$$\frac{d\Delta}{dt} = \frac{d\nu}{dt} = 0 \tag{9}$$

for parcels on an inviscid adiabatic flow. Since number densities are more commonly considered in tracer studies, we shall work in terms of ν rather than Δ in subsequent analysis.

b. Perturbations due to adiabatic vertical displacements

Next we consider local responses of each conserved term to a small vertical adiabatic displacement ζ of an air parcel from its equilibrium position z_1 to a new height

$$z_2 = z_1 + \zeta, \tag{10}$$

given the standard background pressure profile

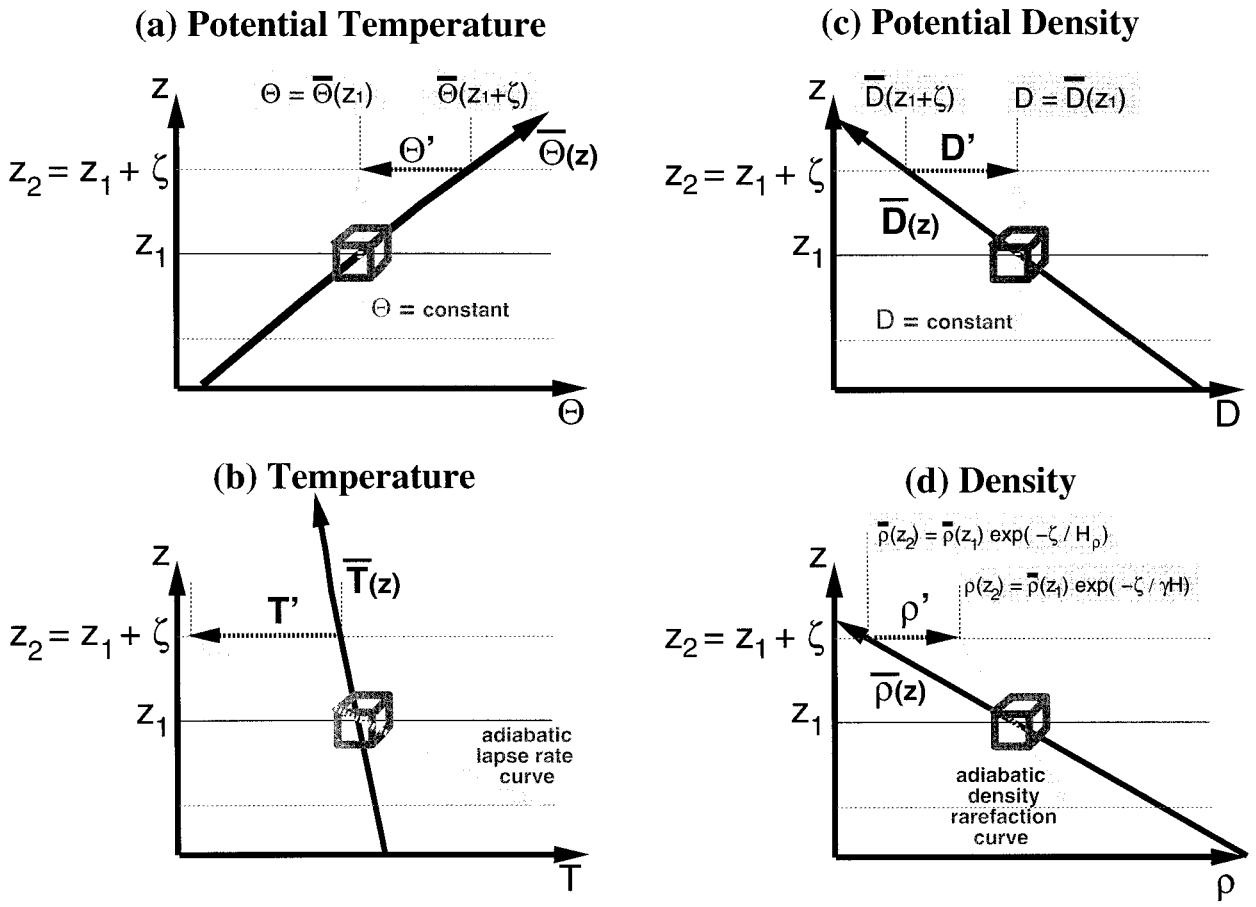

FIG. 1. Schematic diagram of response (light dotted curve) of (a) potential temperature Θ, (b) absolute temperature T, (c) potential density D, and (d) absolute density ρ in an air parcel (shown as a cube) as it is adiabatically advected a small vertical distance ζ from its equilibrium rest position z_1, where it is in thermal equilibrium with the background atmosphere. Background profiles of each quantity are plotted with solid curves.

$$\overline{p}(z_2) = \overline{p}(z_1)\exp\left(\int_{z_1}^{z_2}\frac{-dZ}{H(Z)}\right)$$

$$\approx \overline{p}(z_1)\exp\left(\frac{-\zeta}{H(z_1)}\right), \qquad (11)$$

where $H(z_1) = R\overline{T}(z_1)/g$ is the pressure scale height at height z_1, and the latter expression in (11) is sufficiently accurate for small ζ given a background temperature profile $\overline{T}(z)$ that varies slowly with height.

The formal parcel-based analysis of this problem is given in appendix A, where departures (perturbations) of parcel-based quantities from surrounding background values are derived. The basic procedure for computing these perturbations is depicted schematically in Fig. 1 for both temperature and density. In each panel in Fig. 1, an air parcel has been advected from its equilibrium height z_1 to a new height, z_2, and in each case the adiabatic response is given by moving the parcel along the light dotted ''response curve.'' The top panels of Fig. 1 show constructions for the potential temperature and potential density: since both remain constant within the air parcel, their response curves are vertical. Corresponding constructions in terms of the absolute temperature and density are shown in the lower panels. Their response curves are given by $T(z_1, z_2)$ and $\rho(z_1, z_2)$ in (5)–(6): hereafter, it proves expedient to use the abbreviated notation $T(z_2)$ and $\rho(z_2)$ for these expressions since z_1 stays constant and the functional dependence on z_1 is implicit from (10). Background profiles are shown with thick solid curves on each plot. Perturbations are given by the difference between the adiabatically varying value within the parcel and the local background value at height z_2, as shown in Fig. 1. Using the abbreviated notation introduced above, this yields perturbation terms $\Theta'(z_2)$, $D'(z_2)$, $T'(z_2)$, and $\rho'(z_2)$.

Simplified equations for these perturbation terms follow when the displacement ζ is sufficiently small that variations in both the background profiles and the adiabatic response curves between z_1 and z_2 are approximately linear in Fig. 1. This holds so long as any curvature of these profiles occurs over vertical scales $L \gg$

ζ. Since the formal parcel relations in appendix A are height-varying exponentials, L can be conveniently characterized by the scale height H_X of the exponential relation for quantity X, so that $|\zeta/H_X| \ll 1$. When this condition is satisfied, the exponential parcel relations can be accurately approximated by retaining only the first two terms from their MacLaurin series expansions. For temperatures and densities, these truncated MacLaurin series (TMS) relations yield the instantaneous simplified perturbation relations

$$\frac{\rho'(z_2)}{\overline{\rho}(z_2)} = \frac{D'(z_2)}{\overline{D}(z_2)} = -\left(\frac{\Theta'(z_2)}{\overline{\Theta}(z_2)}\right) = -\left(\frac{T'(z_2)}{\overline{T}(z_2)}\right) = \frac{\zeta}{H_D(z_1)} = \frac{N^2(z_1)}{g}\zeta, \tag{12}$$

where

$$H_D(z_1) = H(z_1)\left(\frac{\gamma - 1}{\gamma} + \frac{\partial H(z_1)}{\partial z}\right)^{-1} = \frac{g}{N^2(z_1)} \tag{13}$$

is the potential density scale height (see appendix A). Equation (12) holds for $|\zeta/H_D| \ll 1$.

c. Range of applicability to gravity waves

Next we consider a sinusoidal form for the vertical parcel displacement from z_1:

$$\zeta = \zeta'(x, y, z_1, t) = \hat{\zeta}\sin(kx + ly + mz_1 - \omega t + \varphi), \tag{14}$$

where $\hat{\zeta}$ is the peak vertical displacement amplitude, φ is a (constant) phase offset, (k, l, m) is the wavenumber vector, and ω is the oscillation frequency of the parcel about its equilibrium height z_1. Considering potential temperature only for the moment, (14) and (12) yield

$$\frac{\Theta'(x, y, z_2, t)}{\overline{\Theta}(z_2)} = \frac{-N^2(z_1)}{g}\zeta'(x, y, z_1, t). \tag{15}$$

Since $\hat{\zeta}$ is small ($|\hat{\zeta}/H_D| \ll 1$), replacing the variable term $\overline{\Theta}(z_2)$ with the constant value $\overline{\Theta}(z_1)$ introduces negligible errors in (15). Then, to a good approximation, we can remove the explicit transport of parcels to z_2 so that we can reexpress the potential temperature perturbation (15) as a sinusoidal expression of the form (14) at a fixed height z_1:

$$\Theta'(x, y, z_1, t) = \hat{\Theta}(z_1)\sin(kx + ly + mz_1 - \omega t + \varphi), \tag{16}$$

where

$$\hat{\Theta}(z_1) = \frac{-N^2(z_1)}{g}\overline{\Theta}(z_1)\hat{\zeta} = -\frac{\partial\overline{\Theta}(z_1)}{\partial z}\hat{\zeta}. \tag{17}$$

Transport of parcels to z_2 is now implicit within (16) and (17). Similar relations to (17) follow from (12) and (14) for relative perturbations of potential density, density, and temperature, with peak amplitudes interrelated as

$$\frac{\hat{\rho}}{\overline{\rho}} = \frac{\hat{D}}{\overline{D}} = -\left(\frac{\hat{T}}{\overline{T}}\right) = -\left(\frac{\hat{\Theta}}{\overline{\Theta}}\right) = \frac{N^2}{g}\hat{\zeta}. \tag{18}$$

The relations (14) and (18) have the same form as the simplified polarization relations that govern a hydrostatic gravity wave of intrinsic frequency ω. This occurs because, in the linear hydrostatic limit, a gravity wave advects air parcels adiabatically (e.g., Fritts and Rastogi 1985), has a small displacement amplitude $\hat{\zeta}$ ($|\hat{\zeta}/H_D| \ll 1$), and produces a negligible pressure perturbation within displaced parcels (e.g., Gossard and Hooke 1975).

To assess the degree and range of this correspondence more quantitatively, a standard non-Boussinesq linearized perturbation derivation of the acoustic–gravity wave equations is outlined in appendix B. There it is shown that the parcel-derived polarization relations (18) are an acceptable approximation to the full acoustic–gravity wave polarization relations when the normalized quantities $|a(m, \omega)|$ and $|b(m, \omega)|$ are $\ll 1$ [see Eqs. (B10) and (B11)]. When this limit is not satisfied, wave-induced pressure perturbations become nonnegligible [see Eq. (B13)], so the parcel approach (which assumes zero pressure perturbation) becomes inaccurate. Sample calculations in appendix B show that the differences between the full acoustic–gravity wave polarization relations and the parcel-based approximations (18) are small for $\lambda_z = 2\pi/|m| \lesssim 20$ km (see Figs. B1b and B1c). Thus, we use this as an approximate upper-wavelength bound on the validity of the hydrostatic gravity wave approximation and of subsequent parcel-based derivations of gravity wave–induced minor constituent variability.

3. Gravity wave perturbations of minor constituents

We now apply the parcel-based approach to model gravity-wave-induced perturbations of minor constituent profiles. We begin by considering some simple examples and compare the parcel-based derivations (appendix A) with corresponding equations derived by a conventional linearized perturbation analysis (appendix B).

a. Tracer with linear $\overline{q}(z)$ profile

The parcel-based approach to this problem is depicted schematically in Fig. 2a and yields the perturbation formula (A19). Since the background profile is linear, then $\overline{q}(z_2) = \overline{q}(z_1) + (\partial\overline{q}/\partial z)\zeta'$, whereupon (A19) and the wave solution (14) yield

$$q'(x, y, z_2, t) = -\left(\frac{\partial\overline{q}}{\partial z}\right)\zeta'(x, y, z_1, t). \tag{19}$$

As for (15), if $\hat{\zeta}$ is small, then the explicit transport of parcels to z_2 can be removed in order that (19) can be

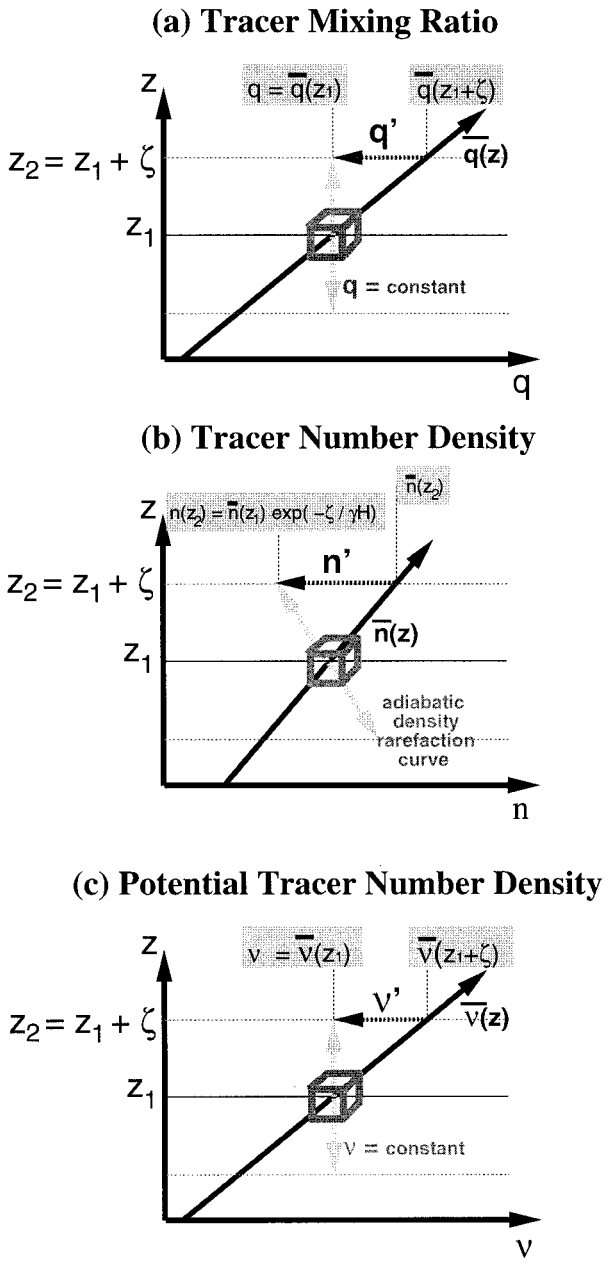

FIG. 2. As in Fig. 1 but for (a) tracer mixing ratio q, (b) tracer number density n, and (c) potential tracer number density ν of the parcel.

reexpressed as a wave solution of the form (16), with peak amplitudes related as

$$\hat{q}(z_1) = -\left(\frac{\partial \overline{q}}{\partial z}\right)\hat{\zeta}. \tag{20}$$

A standard linearized perturbation analysis of (3a) using the methodology in appendix B yields the linearized perturbation mixing ratio equation (e.g., Randel 1990)

$$-\iota\omega\hat{q} + \left(\frac{\partial \overline{q}}{\partial z}\right)\hat{w} = 0, \tag{21}$$

which, since $\hat{w} = -\iota\omega\hat{\zeta}$,, also yields (20) at a given height z_1. Thus the two approaches give identical results in this case.

b. Tracer with a linear $\overline{n}(z)$ profile

The parcel-based approach to this problem is depicted schematically in terms of tracer number density in Fig. 2b and in terms of potential tracer number density in Fig. 2c. The mathematical derivations are set out in appendix A. Because $\overline{n}(z)$ is linear and $\overline{\nu}(z)$ is approximately linear over the interval ζ, then TMS expansions of the parcel relations for tracer perturbations [e.g., (A25b)] are accurate, leading to the simplified TMS result

$$\frac{\nu'(x, y, z_2, t)}{\overline{\nu}(z_2)} = \frac{n'(x, y, z_2, t)}{\overline{n}(z_2)} \approx \frac{\zeta'(x, y, z_1, t)}{H_\nu(z_1)} \tag{22}$$

[see (A26)], where

$$H_\nu(z_1) = -\left(\frac{1}{\gamma H(z_1)} + \frac{1}{\overline{n}(z_1)}\frac{\partial \overline{n}(z_1)}{\partial z}\right)^{-1} \tag{23}$$

is the ''potential tracer density scale height'' by analogy to the potential *total* density scale height (13) [see (A7)]. Since $\overline{n}(z)$ is linear, the accuracy of the TMS relation (22) is controlled only by the curvature of the exponential response curve (A21) shown in Fig. 2b and so is accurate for $|\hat{\zeta}/\gamma H| \ll 1$.

As for (15) and (19), if $\hat{\zeta}$ is small, then the explicit transport of parcels to z_2 can be removed from (22) so that this equation can be reexpressed as a wave solution of the form (16) at the equilibrium height z_1, with peak amplitudes related as

$$\frac{\hat{n}(z_1)}{\overline{n}(z_1)} = -\left[\frac{1}{\gamma H(z_1)} + \frac{1}{\overline{n}(z_1)}\frac{\partial \overline{n}}{\partial z}\right]\hat{\zeta}, \tag{24}$$

where $\partial\overline{n}/\partial z$ is a constant here.

Equation (24) also follows from a linearized perturbation analysis using the nonhydrostatic isothermal acoustic–gravity wave equations of Hines (1960) (Dudis and Reber 1976; Chiu and Ching 1978; Weinstock 1978; Gardner and Shelton 1985; Sugiyama 1988). A similar analysis in appendix B shows that the full expression for nonhydrostatic acoustic–gravity waves is [see (B20)]

$$\frac{\hat{n}(z_1)}{\overline{n}(z_1)} = -\left\{\frac{1}{\gamma H(z_1)} + \frac{1}{\overline{n}(z_1)}\frac{\partial \overline{n}}{\partial z} - \frac{N^2(z_1)}{g}[a(m, \omega) + \iota b(m, \omega)]\right\}\hat{\zeta}. \tag{25}$$

Therefore (24) is valid only when $|a(m, \omega)|$ and $|b(m, \omega)|$ are negligible, which, as discussed in section 1c and

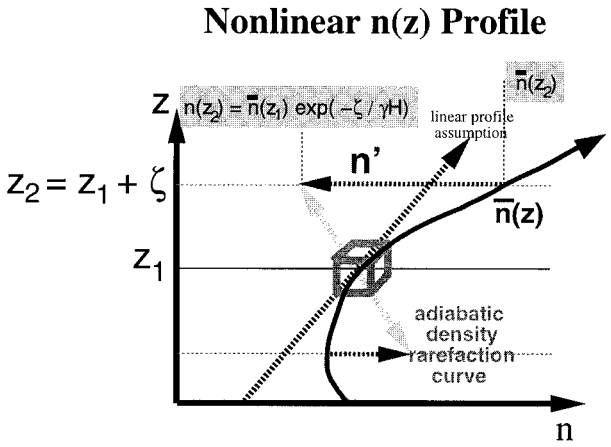

FIG. 3. As in Fig. 2b but illustrating the complications introduced by advecting a parcel across a nonlinear $\overline{n}(z)$ profile.

appendix B, holds only for hydrostatic gravity waves of $\lambda_z \lesssim 20$ km. Thus, (24) is a hydrostatic result (see also Dudis and Reber 1976), despite the fact that nonhydrostatic wave equations are needed to arrive at this result in some linearized perturbation analyses (e.g., Gardner and Shelton 1985). Note that no such caveats applied to the mixing ratio relation (20)—it holds for both hydrostatic and nonhydrostatic waves. Therefore, mixing ratio is the more straightforward quantity to consider when converting between minor constituent perturbations and displacement perturbations due to nonhydrostatic gravity waves or ''tall'' (fast) Kelvin waves.

c. Tracer with a weakly nonlinear $\overline{n}(z)$ profile

Of course tracer density profiles cannot be infinitely linear, but instead usually approximate some type of Chapman curve. If the curvature of the profile is gradual with height, then, for hydrostatic waves, (24) is often used to model wave-induced perturbations, with $\partial\overline{n}(z_1)/\partial z$ reevaluated at each new height z_1 in (24), as in (23) (e.g., Chiu and Ching 1978; Gardner and Voelz 1985; Senft and Gardner 1991). For this to be accurate, the profile needs to be approximately linear only over the limited range $z_1 \pm \hat{\zeta}$, as shown in Fig. 2b. However, this approximation may not always be sufficiently accurate for certain profile shapes, as shown schematically in Fig 3. Thus, tests of its adequacy for a given profile are required.

In the parcel-based approach, the assessment is straightforward. For an exponential $\overline{n}(z)$ profile, for instance, (22) and hence (24) are accurate for $|\hat{\zeta}/H_\nu| \ll 1$, from (A6a) and (A6b). For arbitrary profile shapes, we simply avoid TMS approximations and use the general parcel solution (A21), which, using (14), yields the normalized perturbation relation

$$\frac{n'(x, y, z_2, t)}{\overline{n}(z_2)} = \frac{\overline{n}(z_1)}{\overline{n}(z_2)} \exp\left(\frac{-\zeta'(x, y, z_1, t)}{\gamma H(z_1)}\right) - 1, \quad (26)$$

from (A23b), where $z_2 = z_1 + \zeta'(x, y, z_1, t)$. Note that (26) yields a nonsinusoidal solution. In terms of potential tracer density ν, this is equivalent to using (A6a) or (A8) instead of the approximate relation (A6b). Direct comparison of results using (24) and (26) then indicate whether the former equation is sufficiently accurate for modeling wave perturbations of a given $\overline{n}(z)$ profile.

Such assessments are less straightforward within the framework of a linearized perturbation analysis (e.g., Chiu and Ching 1978). Gardner and Shelton (1985) developed an iterative method for deriving higher-order corrections to (24) due to the curvature of a given $\overline{n}(z)$ profile, using perturbation expansions based on an assumed form for the solution. Their most general solution took the form

$$n(x, y, z, t) = \frac{\overline{n}\left[z - \gamma H(z) \ln\left(1 + \dfrac{A'(x, y, z, t)}{\gamma - 1}\right)\right]}{1 + \dfrac{A'(x, y, z, t)}{\gamma - 1}}, \quad (27)$$

where $A'(x, y, z, t)$ is a normalized gravity wave–induced perturbation, which, for small-amplitude waves in an isothermal atmosphere (Hines 1960), is approximately equal to the relative density perturbation of the wave [see Eq. (38) of Gardner and Shelton 1985]. It then follows that (27) corresponds approximately to the parcel solution (A21) derived in appendix A since $1 + A'(x, y, z, t)/(\gamma - 1) \approx 1 + \zeta'(x, y, z, t)/\gamma H(z)$, which in turn is a TMS expansion of $\exp[\zeta'(x, y, z, t)/\gamma H(z)]$.

Gardner and Shelton converted their solutions into perturbation formulas at a set height z_1 using MacLaurin series expansions. They derived the following extension of (24) in which the effects of both first- and second-order vertical derivatives of $\overline{n}(z)$ were retained:

$$\frac{n'(x, y, z_1, t)}{\overline{n}(z_1)} \approx \frac{-1}{\gamma - 1}\left[1 + \left(\frac{\gamma H(z_1)}{\overline{n}(z_1)}\right)\frac{\partial\overline{n}(z_1)}{\partial z}\right]\frac{\rho'(x, y, z_1, t)}{\overline{\rho}(z_1)} + \frac{1}{(\gamma - 1)^2}\left[1 + \left(\frac{3\gamma H(z_1)}{2\overline{n}(z_1)}\right)\frac{\partial\overline{n}(z_1)}{\partial z} + \left(\frac{\gamma^2 H^2(z_1)}{2\overline{n}(z_1)}\right)\frac{\partial^2\overline{n}(z_1)}{\partial z^2}\right]\left(\frac{\rho'(x, y, z_1, t)}{\overline{\rho}(z_1)}\right)^2, \quad (28)$$

where $\rho'(x, y, z_1, t)$ is the gravity wave density oscillation, which in this case is related to $\hat{\zeta}$ through (14) and (18) using isothermal relations ($\partial H(z_1)/\partial z = 0$) to evaluate $N^2(z_1)$ in (13). Like (26), Eq. (28) is also a nonsinusoidal solution.

In Fig. 4, we compare (28) with the linear profile solution (24) and the parcel solution (26). Since sodium acts as a passive tracer to gravity waves above ~85 km (e.g., Hickey and Plane 1995), we use an $\overline{n}(z)$ profile based on a Gaussian model of the mesospheric sodium layer, similar to the one considered by Gardner and Shelton (1985). The profile is plotted as the thick light curve in Figs. 4b and 4e. We perturb this profile with a hydrostatic gravity wave (14) of vertical wavelength $\lambda_z = 10$ km, $\hat{\zeta} = 800$ m (both representative mesospheric values), and constant phase φ_0. Sample waves are shown in Figs. 4a and 4d as a function of height z at a given location (x_0, y_0) at two different times t. The corresponding perturbations to the background tracer profile are plotted in Figs. 4b and 4e, and the normalized perturbations are isolated and plotted in Figs. 4c and 4f for the parcel solution (26) and the perturbation formulas (24) and (28). The parcel solution (26) is also replotted with a dotted curve in Figs. 4c and 4f at the undisturbed height $z = z_1$, instead of at the perturbed height $z = z_2 = z_1 + \zeta'(x_0, y_0, z_1, t)$ (solid curve), to help separate the deviations that arise due to different physical locations for each parcel (i.e., differences in z_2 and z_1) and those due to incomplete characterization of the effects of mean profile curvature.

We see in Figs. 4c and 4f that the simple relation (24) is reasonably accurate here but that the higher-order correction (28) brings the solution closer to the parcel solution (26). The results in Fig. 4 also show many well-known features of wave-induced fluctuations of tracer number density profiles; for example, that the wave response is always larger on the underside of the layer than on the topside (e.g., Chiu and Ching 1978; Weinstock 1978). This feature is easily appreciated in a parcel analysis by noting that all points on the unperturbed Gaussian profile in Figs. 4b and 4e follow the ''adiabatic rarefaction'' response curve (A21) when vertically advected, as shown in Fig. 2b. This clearly yields greater deviations from the background profile on the bottom side of the layer than on the top side. Also evident in Figs. 4c and 4f is the well-known half-wavelength phase flip across the layer peak (Gardner and Shelton 1985).

d. Tracer with a strongly nonlinear $\overline{n}(z)$ profile

Tracer layers in the middle atmosphere often deviate significantly from the smoothly curved profiles considered in Fig. 4. For example, the mesospheric sodium layer sometimes develops a large narrow spike of enhanced Na density, known as a sudden (or sporadic) sodium layer (SSL) (Clemesha et al. 1980; Kwon et al. 1988; Nagasawa and Abo 1995). Similarly, ozone profiles in the lower stratosphere near the edge of the polar vortex often contain large narrow enhancements or depletions, known as ''laminae'' (e.g., Reid and Vaughan 1991). Neither the linearized perturbation relation (24) nor its second-order correction (28) are sufficiently accurate for modeling wave-induced effects within such profiles.

However, parcel-based methods can be used since they require no prior assumptions about the shape of the background vertical profile. To illustrate this, we simulate an SSL by adding a narrow Gaussian layer to the original Gaussian in Fig. 4, choosing its parameters to resemble the ''typical'' SSL considered by Cox et al. (1993). The resultant profile is the thick light curve shown in each panel of Fig. 5. We perturb this profile with the same wave as in Fig. 4. Solid curves in Fig. 5 show the perturbed profile as calculated using the parcel solution (A21) and the wave oscillation (14), with each panel showing results at six successive equispaced time values t spanning a full wave period $2\pi/\omega$. We see that the SSL is not only advected up and down by the wave, but is also periodically expanded (Fig. 5b) and compressed (Fig. 5e).

Detailed features of the response are more easily seen in surface renderings of successive profiles, shown in Fig. 6. Figure 6a shows the periodic oscillation of the SSL peak and the downward movement of wave phase fronts above and below the SSL, the latter associated with an approximately linear wave response within the basic Gaussian profile (Figs. 4c and 4f). The SSL is focused upon in Fig. 6b, which shows a sinusoidal advection of its peak value and periodic contraction and expansion of its width.

Figure 7 shows a representative lower-stratospheric ozone profile with a lamina superimposed (thick light curve), based on the lidar observations of Gibson-Wilde et al. (1997). Like sodium, ozone has a long chemical lifetime at these heights and therefore acts as a tracer to gravity wave motions. We perturb the profile with a gravity wave of $\hat{\zeta} = 200$ m and $\lambda_z = 2.3$ km, choices based on the gravity wave detected and characterized by Gibson-Wilde et al. (1997) at ~12–18 km during their ozone measurement. Parcel results using (A21) for a full wave cycle are shown with solid curves in Fig. 7. Again, we see not only vertical advection of the lam-

→

FIG. 4. Perturbations of a Gaussian number density profile $\overline{n}(z)$ [thick light curve in (b) and (e)] are plotted in (b) and (e), as produced by the gravity wave shown above it in (a) and (d), respectively. Corresponding relative perturbations are plotted below in (c) and (f). Results using parcel advection methods (solid and dotted curves) are compared to the results (24) (dashed curve) and (28) (broken curve) based on linearized perturbation solutions. The thick light curves in (c) and (f) show the asymmetric amplitude envelope of the parcel solution, given from (A23a) by $[\overline{n}(z)/\overline{n}(z \pm \hat{\zeta})] \exp(\mp\hat{\zeta}/\gamma H) - 1$. An isothermal atmosphere of $H = 7$ km was used.

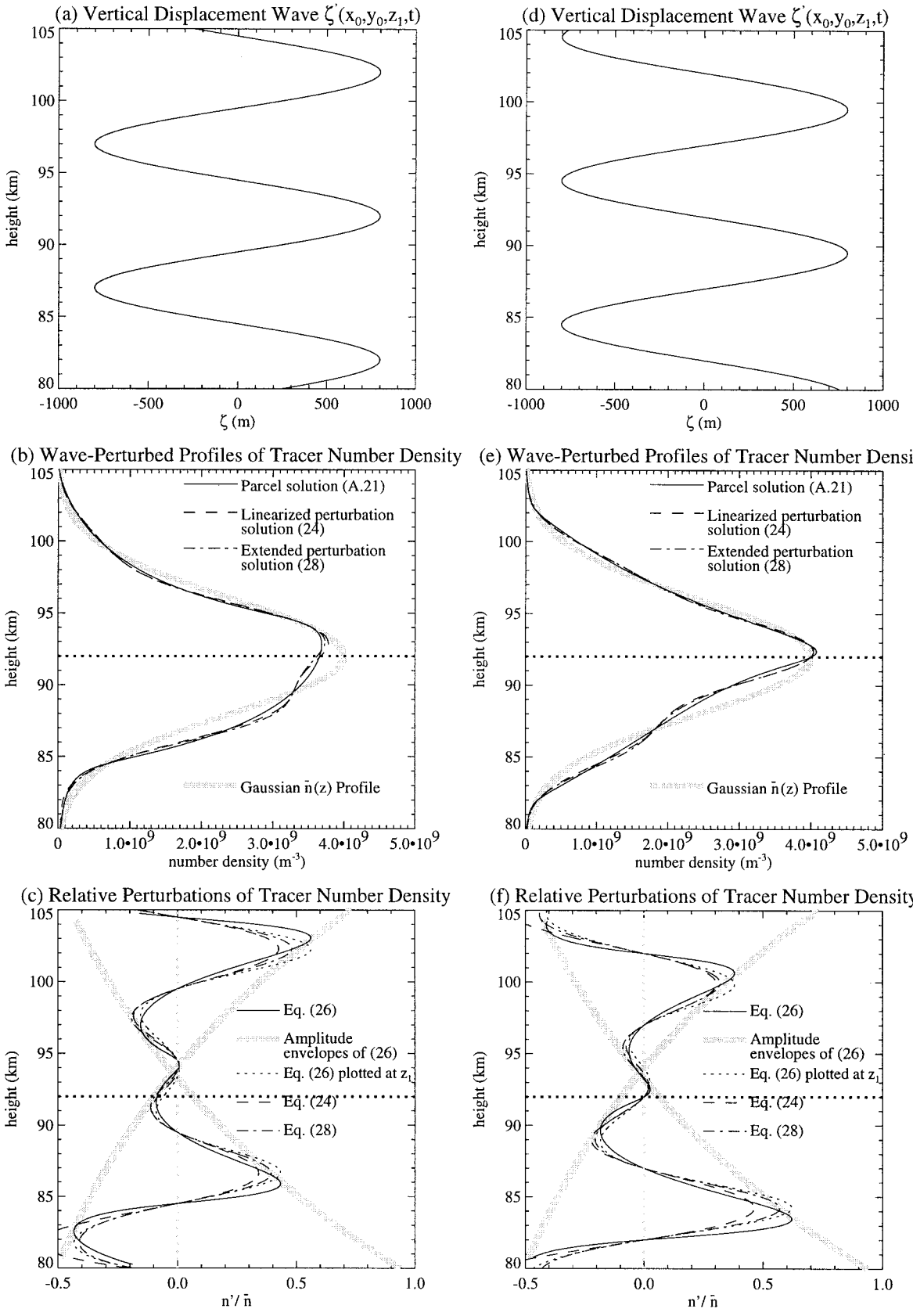

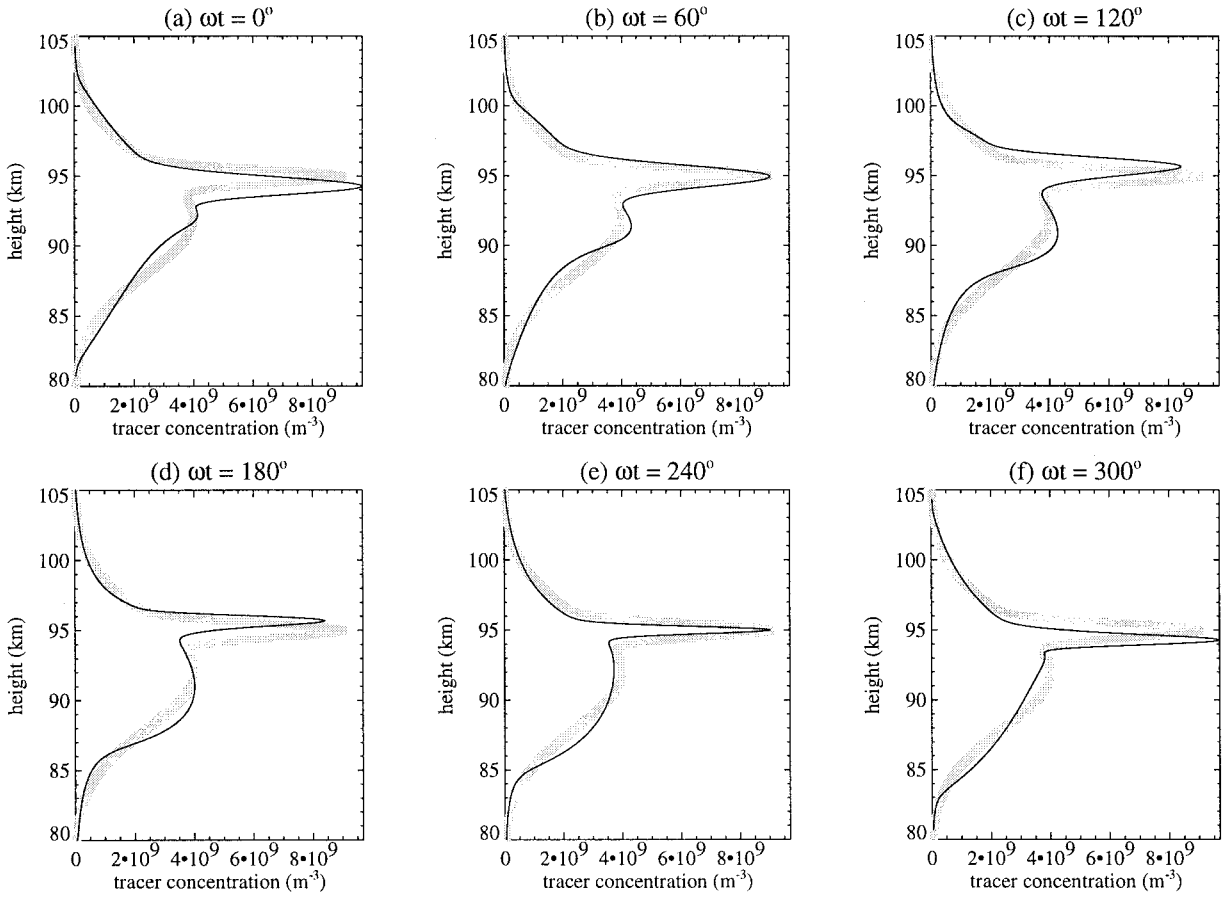

FIG. 5. Sequence of six profiles (at equispaced times t spanning one wave period) of a wave-perturbed Na layer (solid curve) as in Fig. 4, but with an SSL inserted at 95 km (based on Fig. 1 of Cox et al. 1993). The thick light curve shows the unperturbed profile in each case.

ina, but compression and expansion of its width as well, features that are more obvious in the corresponding surface plot in Fig. 8. Effects such as these may account for some of the standard deviation in mean magnitudes and widths of ozone laminae found in collated ozonesonde data (e.g., Fig. 7 of Reid and Vaughan 1991), as well as variability of other narrow atmospheric layers: for example, tropospheric chemical layers (Newell et al. 1996), cloud structures (e.g., Carslaw et al. 1998), polar mesosphere summer echoes (e.g., Fig. 1 of Rüster et al. 1996), and stratospheric aerosols (Shibata et al. 1994; Hansen and Hoppe 1997). Figure 8 also shows the regular downward movement of wave phase fronts above and below the lamina, where the response approximates a linear wave solution of the form (24).

e. Three-dimensional gravity wave advection of a tracer

The features that produce laminated ozone profiles tend to occur in long narrow streamers of meandering air, which lead to large background ozone gradients not only vertically, but also horizontally (e.g., Waugh et al. 1994; Orsolini et al. 1997). These gradients can be important when attempting to isolate wave-related structures in ozone measured within such environments (e.g., Danielsen et al. 1991; Teitelbaum et al. 1996; Bacmeister et al. 1997; Gibson-Wilde et al. 1997). Again, the approximate relations (24) and (28) cannot accurately simulate the effects of gravity waves on such three-dimensional tracer distributions.

The parcel-based theory in appendix A assumed no horizontal gradients in the background tracer profile and cannot be directly applied here. However, the analysis is easily extended to accommodate full three-dimensional wave-induced displacements $[\chi'(x_i, y_i, z_i, t), \eta'(x_i, y_i, z_i, t), \zeta'(x_i, y_i, z_i, t)]$ of a collection of parcels, i ($i = 1, 2, 3, \cdots$) at equilibrium positions (x_i, y_i, z_i) within an arbitrary three-dimensional tracer distribution $\overline{q}(x, y, z)$.

The mixing ratio response (A19) generalizes to

$$q[x_i + \chi'(x_i, y_i, z_i, t), y_i + \eta'(x_i, y_i, z_i, t), z_i + \zeta'(x_i, y_i, z_i, t)] = \overline{q}(x_i, y_i, z_i), \quad (29)$$

which, as discussed in section 3b, holds for hydrostatic

and nonhydrostatic waves. If we can assume that background isentropic surfaces are horizontal, then a corresponding extension of (A21) yields the number density response

$$n[x_i + \chi'(x_i, y_i, z_i, t), y_i + \eta'(x_i, y_i, z_i, t), z_i + \zeta'(x_i, y_i, z_i, t)] = \overline{n}(x_i, y_i, z_i) \exp\left(\frac{-\zeta'(x_i, y_i, z_i, t)}{\gamma H(z_i)}\right) \quad (30)$$

for a background number density distribution $\overline{n}(x, y, z)$.

As discussed in section 3b, (30) is accurate for hydrostatic gravity waves only. In environments where large narrow horizontal gradients in background potential temperatures/densities also arise, additional compression and expansion occurs as parcels are horizontally advected by the wave. In this situation, not only must the exponential in (30) be modified to account for this extra horizontal compression/expansion, but extended wave equations may be needed that incorporate concomitant modifications to the wave motion (e.g., Lamb and Shore 1992). Since background isentropes rarely tilt from the horizontal by more than a few degrees, then (30) should adequately describe gravity wave–induced perturbations of a three-dimensional distribution of tracer number densities in most circumstances.

It should be noted that the parcel relations (29) and (30) are Lagrangian expressions. A typical application, then, would be in supplementing synoptic-scale parcel advection models with oscillatory gravity wave advection effects (e.g., Pierce et al. 1994). The Eulerian tracer perturbations that such simulations will produce (e.g., fluctuations in vertical tracer profiles) will be quite complicated in general.

f. Gravity wave perturbations of shorter-lived constituents

The parcel-based approach can also be used for shorter-lived constituents. We illustrate this by using it to reproduce some well-known results for ozone.

While the lower-stratospheric ozone in Figs. 7–8 acts as a tracer, the ozone production/loss term in (1b), R_{O_3}, becomes nonnegligible above ~25–30 km. Assuming Chapman photochemistry, then

$$R_{O_3} \approx 2J_{O_2}n_{O_2} - \frac{2k_{O_3}J_{O_3}n_{O_3}^2}{k_{O_2}n_M n_{O_2}}, \quad (31)$$

where n_x is the number density of constituent x, J_x is its photolysis rate, and k_x is its recombination rate (Brasseur and Solomon 1984). As shown in appendix C, applying a parcel-based analysis to (2) and (31) yields a linearized response of the photochemical term R_{O_3} to an adiabatic vertical displacement of the parcel of the form

$$\frac{dq_{O_3}(z_2)}{dt} = -\overline{B}(z_2)q'_{O_3}(z_2) - \overline{C}(z_2)T'(z_2), \quad (32)$$

for small vertical displacements ζ, where $q_{O_3}(z_2) = \overline{q}_{O_3}(z_2) + q'_{O_3}(z_2)$ from (A19) and $T'(z_2)$ is the TMS temperature perturbation (A13). Since $\overline{R}_{O_3}(z) \approx 0$, then, for a linear $\overline{q}(z)$ profile,

$$\frac{d\overline{q}_{O_3}(z_2)}{dt} = \left(\frac{\partial \overline{q}_{O_3}}{\partial z}\right) w(z_2), \quad (33)$$

where $w(z_2) = d\zeta/dt$ is the vertical velocity of the parcel at z_2 (see Fig. 2a). Thus (32) and (33) yield

$$\frac{dq'_{O_3}(z_2)}{dt} + w(z_2)\left(\frac{\partial \overline{q}_{O_3}}{\partial z}\right) = -\overline{B}(z_2)q'_{O_3}(z_2) - \overline{C}(z_2)T'(z_2). \quad (34)$$

This equation was first derived by Lindzen and Goody (1965) using a linearized perturbation expansion of (2) and (31).

We now substitute the wave solution (14). If $\hat{\zeta}$ is small and the vertical variation of background quantities in (34) is gradual (as assumed in appendix C) and approximately linear over the interval $z_1 \pm \hat{\zeta}$, then explicit parcel transport to z_2 can be removed so that the linearized mixing ratio and temperature perturbations in (34) can also be expressed as wave solutions of the form (14) and (16). Substitution of those solutions into (34) yields, with the help of (21), (A5), and (13), the peak amplitude relation

$$\left(1 - \iota\frac{\overline{B}(z_1)}{\omega}\right)\hat{q}_{O_3}(z_1) = \left(\frac{\partial \overline{q}_{O_3}(z_1)/\partial z}{\partial \overline{T}(z_1)/\partial z + \Gamma_a} + \iota\frac{\overline{C}(z_1)}{\omega}\right) \times \hat{T}(z_1), \quad (35)$$

where Γ_a is the dry-adiabatic lapse rate. This is the basic ozone–temperature relation derived for Kelvin waves by Randel (1990). It illustrates the two limiting cases of the response. For $\omega^2 \gg \overline{B}^2$ and $(\overline{C}/\omega)^2 \ll [(\partial \overline{q}_{O_3}/\partial z)/(\partial \overline{T}/\partial z + \Gamma_a)]^2$, terms on the right of (34) are small while terms on the left are large and dominate, so (35) approximates the tracer solution (20). For $\omega^2 \ll \overline{B}^2$ and $(\overline{C}/\omega)^2 \gg [(\partial \overline{q}_{O_3}/\partial z)/(\partial \overline{T}/\partial z + \Gamma_a)]^2$, photochemistry dominates so that terms on the right-hand side of (34) are much larger than the parcel transport terms on the left. In this latter case, (35) tends toward the photochemistry-dominant limit

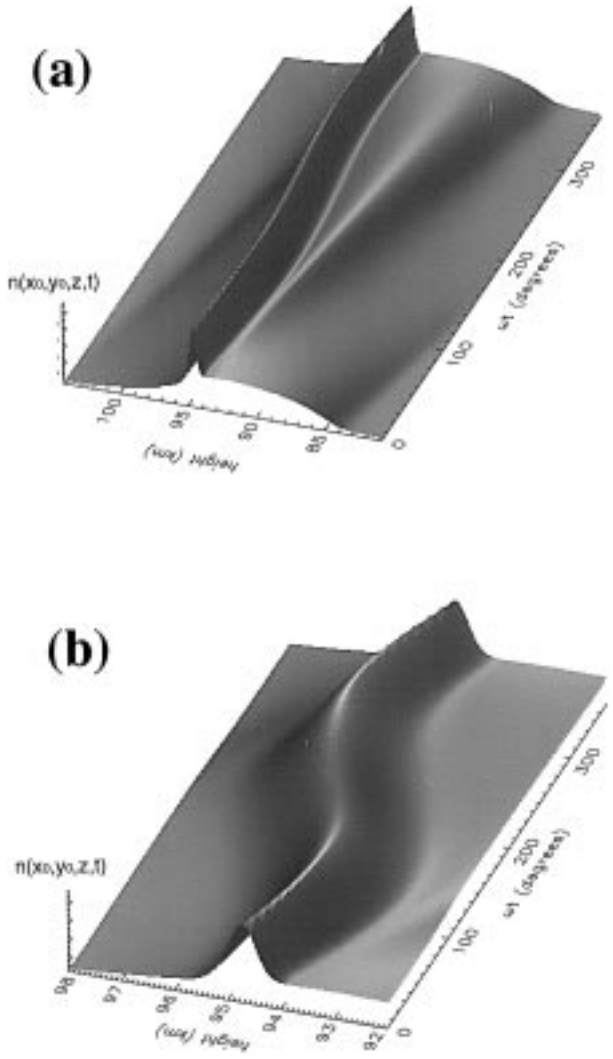

FIG. 6. Time–height surface rendering of the perturbed Na number density response in Fig. 5. Both plots span one wave period. Panel (a) shows variations over the full height range of the Na layer, while (b) focuses on the SSL.

$$\hat{q}(z_1) = -\left(\frac{\overline{C}(z_1)}{\overline{B}(z_1)}\right)\hat{T}(z_1), \tag{36}$$

which also follows on setting the left-hand side of (34) to zero.

This parcel-based analysis assumes adiabatic parcel motion, whereas the perturbation $q'_{O_3}(z_2)$ also produces a diabatic heating/cooling perturbation in the potential temperature equation. However, Zhu and Holton (1986) show that this leads to very minor departures from adiabaticity for hydrostatic gravity waves. Thus parcel-based analyses also work well in simulating (hydrostatic) gravity wave–induced perturbations of constituents with short chemical lifetimes, so long as the perturbed chemical response does not lead to significant diabatic damping of the wave; otherwise, a linearized perturbation analysis should be pursued (e.g., Zhu and Holton 1986).

4. Summary and conclusions

This study has formalized the parcel advection method, applied it to gravity waves, and compared its findings with standard results from linearized perturbation expansions of the governing equations. The combined results of section 3 have shown that the two approaches are equivalent in most circumstances. However, we also identified certain situations in which one or the other method gave more accurate results.

The parcel-based method becomes inaccurate when simulating perturbations of tracer density profiles by nonhydrostatic gravity waves. For shorter-lived constituents, the parcel method also becomes inaccurate if the wave-induced photochemical response produces a significant diabatic feedback on the wave. In these instances, the results from traditional linearized perturbation analysis should be used instead.

On the other hand, the parcel-based approach is the better method for modeling hydrostatic gravity wave perturbations of tracers with sharp spatial gradients in their background distribution. We illustrated this by using it to model wave-induced modulations of sporadic sodium layers and ozone laminae (Figs. 5–8).

While we have restricted attention here to gravity waves, the parcel methodology described here can also be applied to other types of waves, such as free and forced Rossby waves, mixed Rossby–gravity waves, Kelvin waves, and tides. For some of these waves, both meridional and vertical wave displacements are necessary to simulate their effects on tracers (e.g., Randel 1993; Stanford and Ziemke 1993). Parcel advection models have already been used extensively to simulate the effects of stationary Rossby waves on stratospheric tracer distributions.

Acknowledgments. Thanks to Mary Anderson, Andrea Hollin, Jane Ford, DuRene Brimer, and ''Chap'' Chappell at Computational Physics, Inc., and Mary-Ann Lindsey at the Naval Research Laboratory, Washington, D.C., for their help with the administration and public release of this paper. Thanks also to Chet Gardner, Richard Walterscheid, and an anonymous reviewer for helpful comments on the manuscript. SDE also thanks Colin Hines for comments on an earlier draft and for helping to resolve SDE's misunderstandings of some of his earlier work. This research was partially supported by the Office of Naval Research, Washington, D.C., and Contract NAS5-97247 of NASA's Atmospheric Effects of Aviation/Subsonic Assessment Program.

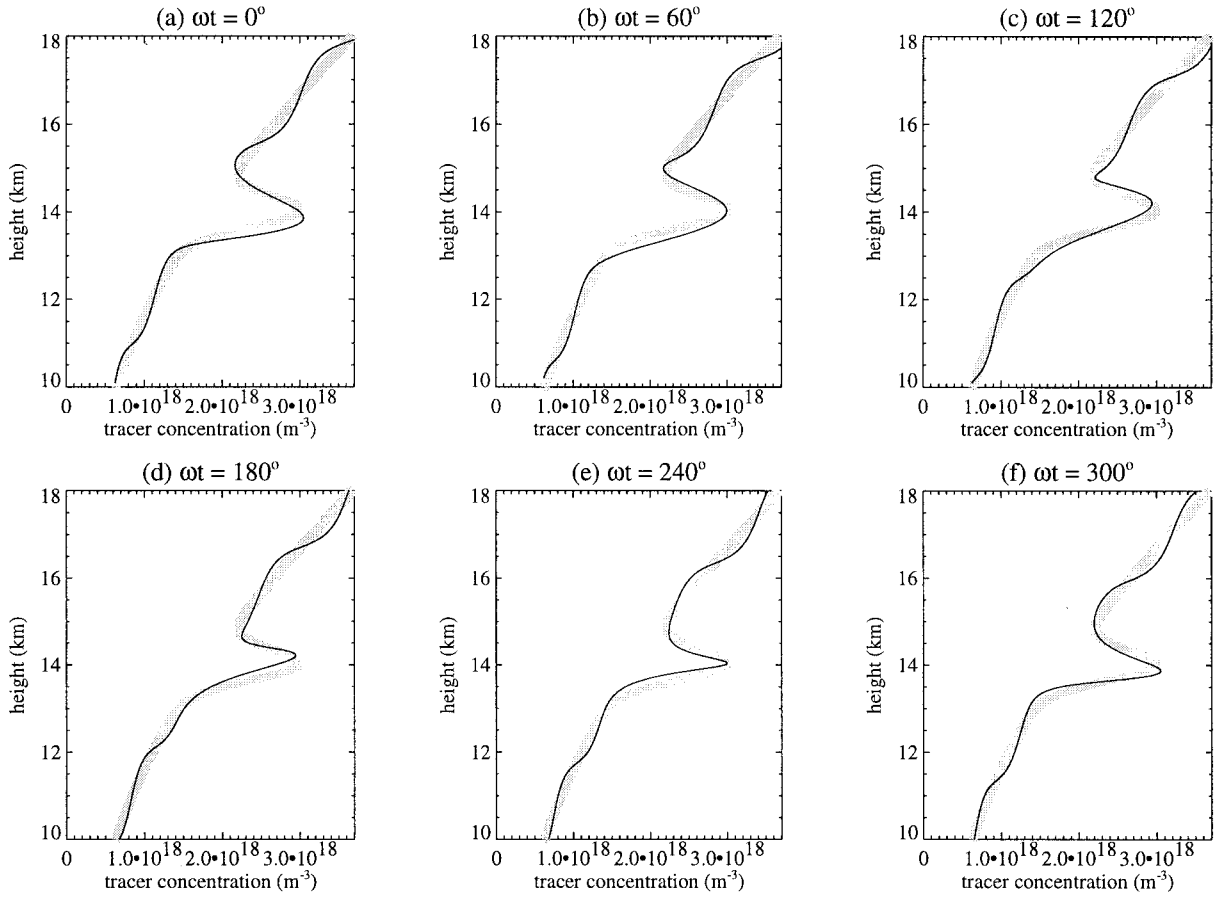

FIG. 7. As in Fig. 5 but using a representation of the ozone layer based on the data of Gibson-Wilde et al. (1997), with a lamina at 14 km. Thick light curves show the unperturbed profile. Solid curves show perturbed profiles due to a gravity wave of $\lambda_z = 2.3$ km and $\hat{\zeta} = 200$ m.

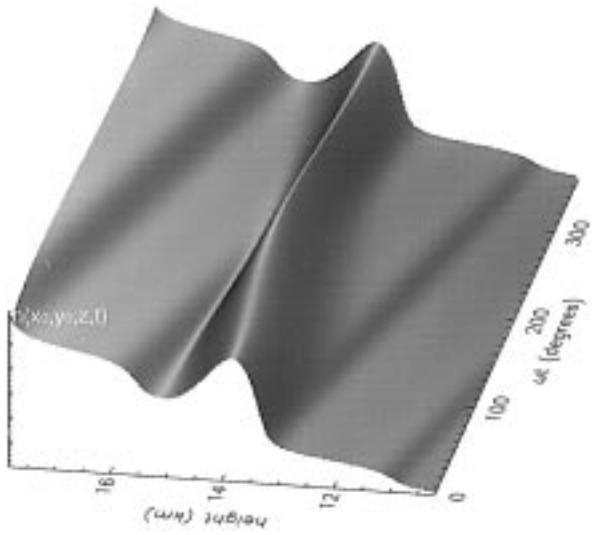

FIG. 8. As in Fig. 6a but showing the ozone number density response from Fig. 7.

APPENDIX A

Perturbation Formulas Using the Parcel Methodology

a. Background profiles

The ideal gas law and the altimeter equation (11) yield the standard background density relation

$$\overline{\rho}(z_2) = \overline{\rho}(z_1)\frac{\overline{T}(z_1)}{\overline{T}(z_2)}\exp\left(\frac{-\zeta}{H(z_1)}\right) \approx \overline{\rho}(z_1)\exp\left(\frac{-\zeta}{H_\rho(z_1)}\right), \tag{A1}$$

where

$$H_\rho(z_1) \approx H(z_1)\left(1 + \frac{\partial H(z_1)}{\partial z}\right)^{-1} \tag{A2}$$

is the density scale height. On invoking (5) and (6) at z_1 and z_2, then, with the aid of (11), (A1) and (A2), background potential temperature varies with height as

$$\overline{\Theta}(z_2) = \overline{\Theta}(z_1)\frac{\overline{T}(z_2)}{\overline{T}(z_1)}\exp\left(\frac{(z_2 - z_1)(\gamma - 1)}{\gamma H(z_1)}\right) \quad \text{(A3a)}$$

$$\approx \overline{\Theta}(z_1)\exp\left(\frac{\zeta}{H_D(z_1)}\right), \quad \text{(A3b)}$$

while background potential density varies with height as

$$\overline{D}(z_2) = \overline{D}(z_1)\frac{\overline{\rho}(z_2)}{\overline{\rho}(z_1)}\exp\left(\frac{(z_2 - z_1)}{\gamma H(z_1)}\right) \quad \text{(A4a)}$$

$$\approx \overline{D}(z_1)\exp\left(\frac{-\zeta}{H_D(z_1)}\right), \quad \text{(A4b)}$$

where

$$H_D(z_1) = H(z_1)\left(\frac{\gamma - 1}{\gamma} + \frac{\partial H(z_1)}{\partial z}\right)^{-1} = \frac{g}{N^2(z_1)} \quad \text{(A5)}$$

is the potential density scale height, g is gravitational acceleration, and $N(z_1)$ is the background Brunt–Väisälä frequency at height z_1.

From (8), analogous relations for the background potential number density of a given passive trace constituent are

$$\overline{\nu}(z_2) = \overline{\nu}(z_1)\frac{\overline{n}(z_2)}{\overline{n}(z_1)}\exp\left(\frac{(z_2 - z_1)}{\gamma H(z_1)}\right) \quad \text{(A6a)}$$

$$\approx \overline{\nu}(z_1)\exp\left(\frac{-\zeta}{H_\nu(z_1)}\right), \quad \text{(A6b)}$$

where

$$H_\nu(z_1) = -H(z_1)\left(\frac{1}{\gamma} + \frac{H(z_1)}{\overline{n}(z_1)}\frac{\partial \overline{n}(z_1)}{\partial z}\right)^{-1} \quad \text{(A7)}$$

is the potential tracer density scale height. The simplified relation (A6b) is accurate when height variations of the $\overline{n}(z_1)$ profile are approximately exponential over the interval ζ. For small ζ, (A6b) is a good approximation whenever $\overline{n}(z)$ varies over a typical vertical length scale $L \gg \zeta$. However, while background temperatures in (A1) and background densities in (A4a) usually obey such conditions, $\overline{n}(z)$ profiles in (A6a) often do not (see sections 3c and 3d), whereupon (A6a) or the integrated expression

$$\overline{\nu}(z_2) \approx \overline{\nu}(z_1)\exp\left(\int_{z_1}^{z_2 = z_1 + \zeta}\frac{-dZ}{H_\nu(Z)}\right) \quad \text{(A8)}$$

must be used. Note that the reformulation of (A6a) into a fully exponential form (A6b) and (A8) is similar to the approach taken by Lindzen (1981) in parameterizing the variation with height of WKB gravity wave equations [see his Eqs. (11) and (12)].

b. Temperature perturbations

Figure 1a constructs the perturbation of potential temperature produced by the adiabatic vertical displacement ζ of an air parcel from its equilibrium position z_1, as discussed in section 2b. Since Θ in the parcel is conserved, the displacement produces a perturbation from the background profile at height z_2 of

$$\Theta'(z_2) = \overline{\Theta}(z_1) - \overline{\Theta}(z_2). \quad \text{(A9)}$$

From (A3b) and (A5), this implies a normalized perturbation:

$$\frac{\Theta'(z_2)}{\overline{\Theta}(z_2)} = \exp\left(\frac{-\zeta}{H_D(z_1)}\right) - 1 \quad \text{(A10a)}$$

$$\approx \frac{-\zeta}{H_D(z_1)} = \frac{-N^2(z_1)}{g}\zeta$$

$$= -\frac{1}{\overline{\Theta}(z_1)}\frac{\partial \overline{\Theta}(z_1)}{\partial z}\hat{\zeta}, \quad \text{(A10b)}$$

where (A10b) follows from retaining the first two terms of the MacLaurin series expansion of the exponential in (A10a) and is accurate for small ζ (i.e., $|\zeta/H_D(z_1)| \ll 1$). This simplification is referred to hereafter as a truncated MacLaurin series (TMS) expansion and from (A10b) is clearly accurate when the background profile $\overline{\Theta}(z)$ is approximately linear between z_1 and z_2.

The absolute temperature response is depicted in Fig. 1b. Using (5) and (11), the temperature of the displaced parcel becomes

$$T(z_2) = \overline{T}(z_1)\exp\left(\frac{-\zeta(\gamma - 1)}{\gamma H(z_1)}\right) \quad \text{(A11a)}$$

$$\approx \overline{T}(z_1) - \frac{\zeta g}{C_p}, \quad \text{(A11b)}$$

where C_p is the mass specific heat at constant pressure. Equation (A11b) follows from a TMS expansion of (A11a) and reproduces the familiar result that the parcel temperature varies according to the (dry) adiabatic lapse rate $\Gamma_a = g/C_p$ for small ζ. This yields a temperature perturbation

$$T'(z_2) = T(z_2) - \overline{T}(z_2) \quad \text{(A12)}$$

and a relative perturbation, according to (A5), (A11a), and (A12), of

$$\frac{T'(z_2)}{\overline{T}(z_2)} = \frac{\overline{T}(z_1)}{\overline{T}(z_2)}\exp\left(\frac{-\zeta(\gamma - 1)}{\gamma H(z_1)}\right) - 1$$

$$\approx \exp\left(\frac{-\zeta}{H_D(z_1)}\right) - 1$$

$$\approx \frac{-\zeta}{H_D(z_1)} = \frac{-N^2(z_1)}{g}\zeta, \quad \text{(A13)}$$

using a TMS expansion of the exponential. Thus the

relative perturbations of absolute and potential temperature are equal for small ζ.

c. Density perturbations

Figure 1c constructs the perturbation of potential density produced by the same adiabatic vertical displacement ζ of an air parcel from its equilibrium position z_1. Since D in the parcel is conserved, then, as in (A9),

$$D'(z_2) = \overline{D}(z_1) - \overline{D}(z_2). \tag{A14}$$

From (A4b) and (A5), (A14) implies a normalized perturbation,

$$\frac{D'(z_2)}{\overline{D}(z_2)} = \exp\left(\frac{\zeta}{H_D(z_1)}\right) - 1 \tag{A15a}$$

$$\approx \frac{\zeta}{H_D(z_1)} = \frac{N^2(z_1)}{g}\zeta, \tag{A15b}$$

where (A15b) follows from a TMS expansion of (A15a).

Figure 1d shows the corresponding construction for the density perturbation. Using (6) and (11), the density of the adiabatically displaced parcel responds according to

$$\rho(z_2) = \overline{\rho}(z_1)\exp\left(\frac{-\zeta}{\gamma H(z_1)}\right), \tag{A16}$$

which, by analogy to the adiabatic lapse rate for temperature (A11b), we refer to here as the adiabatic rarefaction curve. This yields a density perturbation

$$\rho'(z_2) = \rho(z_2) - \overline{\rho}(z_2), \tag{A17}$$

which, with the aid of (A1), (A2), (A5), and (A16), yields to a relative density perturbation of

$$\frac{\rho'(z_2)}{\overline{\rho}(z_2)} = \frac{\rho(z_2)}{\overline{\rho}(z_2)} - 1$$

$$= \exp\left(\frac{\zeta}{H_D(z_1)}\right) - 1 \tag{A18a}$$

$$\approx \frac{\zeta}{H_D(z_1)} = \frac{N^2(z_1)}{g}\zeta, \tag{A18b}$$

using a TMS expansion of (A18a).

d. Tracer perturbations

Figure 2a constructs the perturbation mixing ratio q' induced by the adiabatic vertical displacement ζ of a parcel from its equilibrium height z_1 in an atmosphere containing a tracer with a background vertical profile $\overline{q}(z)$. Since q in the parcel is conserved according to (3), then

$$q'(z_2) = q(z_2) - \overline{q}(z_2)$$

$$= \overline{q}(z_1) - \overline{q}(z_2) \tag{A19}$$

and

$$\frac{q'(z_2)}{\overline{q}(z_2)} = \frac{\overline{q}(z_1)}{\overline{q}(z_2)} - 1. \tag{A20}$$

Since $\rho = Mn_M$, then (3b) and (A16) imply

$$n(z_2) = \overline{q}(z_1)n_M(z_2)$$

$$= \overline{n}(z_1)\exp\left(\frac{-\zeta}{\gamma H(z_1)}\right), \tag{A21}$$

where $\overline{n}(z)$ is the background number density profile of the tracer. Thus, like the total density ρ in (A16), the tracer number density n responds to adiabatic vertical displacements according to its adiabatic rarefaction curve (A21). As shown in Fig. 2b, this produces a perturbation of tracer number density

$$n'(z_2) = n(z_2) - \overline{n}(z_2), \tag{A22}$$

whose relative magnitude is given by

$$\frac{n'(z_2)}{\overline{n}(z_2)} = \frac{n(z_2)}{\overline{n}(z_2)} - 1$$

$$= \frac{\overline{n}(z_1)}{\overline{n}(z_2)}\exp\left(\frac{-\zeta}{\gamma H(z_1)}\right) - 1 \tag{A23a}$$

$$= \frac{\overline{q}(z_1)}{\overline{q}(z_2)}\exp\left(\frac{\zeta}{H_D(z_1)}\right) - 1 \tag{A23b}$$

$$= \frac{q'(z_2)}{\overline{q}(z_2)} + \frac{\rho'(z_2)}{\overline{\rho}(z_2)} + \left(\frac{q'(z_2)}{\overline{q}(z_2)}\right)\left(\frac{\rho'(z_2)}{\overline{\rho}(z_2)}\right), \tag{A23c}$$

where (A23c) is derived from (A23b) using (A18a) and (A20).

An equivalent derivation in terms of potential tracer number density is shown in Fig. 2c. Since ν in the parcel is conserved, then

$$\nu'(z_2) = \overline{\nu}(z_1) - \overline{\nu}(z_2), \tag{A24}$$

which, with the aid of (8), (11), and (A23a), yields

$$\frac{\nu'(z_2)}{\overline{\nu}(z_2)} = \frac{\overline{\nu}(z_1)}{\overline{\nu}(z_2)} - 1 \tag{A25a}$$

$$= \frac{\overline{n}(z_1)}{\overline{n}(z_2)}\exp\left(\frac{-\zeta}{\gamma H(z_1)}\right) - 1 \tag{A25b}$$

$$= \frac{n'(z_2)}{\overline{n}(z_2)}. \tag{A25c}$$

If ζ is small and $\overline{\nu}(z)$ variations are of much longer vertical scale than ζ, then (A25c) can be simplified using a TMS expansion of (A6b), along with (A7) and (A25a), to yield

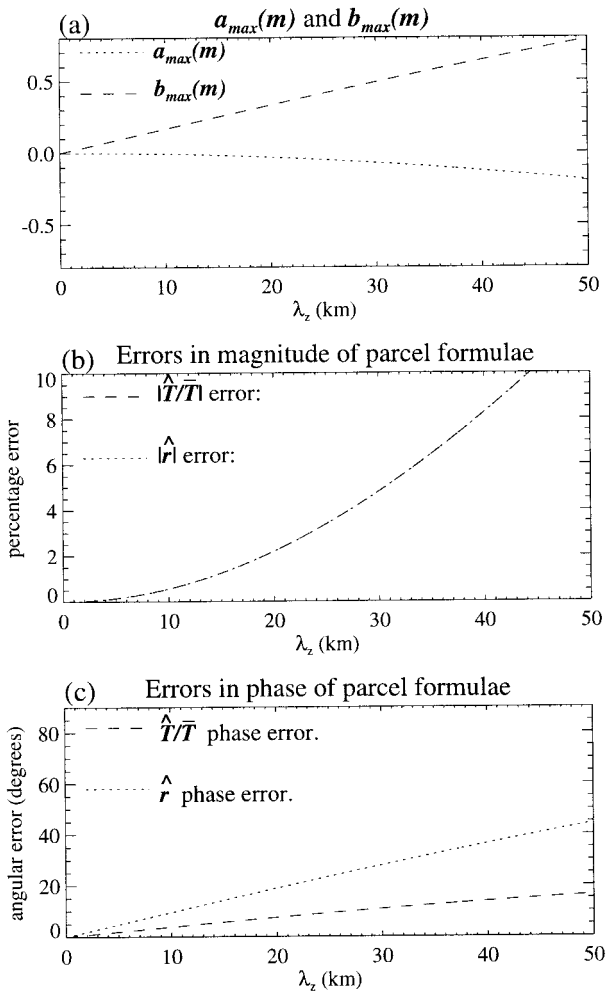

FIG. B1. Vertical wavelength variation of $a_{max}(m)$ and $b_{max}(m)$ (a), and deviations in magnitude (b) and phase (c) between the acoustic–gravity wave polarization relation (appendix B) and the corresponding parcel-based approximation (appendix A) relating $\hat{\zeta}$ to perturbations in relative temperature (dashed line) and relative density (dotted line).

$$\frac{\nu'(z_2)}{\overline{\nu}(z_2)} = \frac{n'(z_2)}{\overline{n}(z_2)} \approx \frac{\zeta}{H_\nu(z_1)}. \tag{A26}$$

The same expression also results from a direct TMS expansion of (A23a). Note the similar forms of (A26) and (A15b).

APPENDIX B

Acoustic–Gravity Wave Polarization Relations

On splitting atmospheric field variables into the sum of a mean and perturbation term ($X = \overline{X} + X'$), isolating and linearizing perturbation terms, and assuming wave solutions of the form

$$X' = \hat{X}\exp[\iota(kx + Mz - \Omega t)] \tag{B1}$$

$$= \hat{X}\exp[\iota(kx + mz - \Omega t) + z/2H_\rho], \tag{B2}$$

the following perturbation equations govern a zonally propagating nonhydrostatic gravity wave in a compressible rotating unsheared inviscid atmosphere (e.g., Gossard and Hooke 1975):

$$-\iota\omega\hat{u} - f\hat{v} = -\iota k\hat{\Phi}, \tag{B3}$$

$$-\iota\omega\hat{v} + f\hat{u} = 0, \tag{B4}$$

$$-\iota\omega\hat{w} + \hat{r}g = -(\iota M - H_\rho^{-1})\hat{\Phi}, \tag{B5}$$

$$-\iota\omega\hat{r} - \left(\frac{N^2}{g}\right)\hat{w} = -\left(\frac{\iota\omega}{c_s^2}\right)\hat{\Phi}, \tag{B6}$$

$$-\iota\omega\hat{r} + \iota k\hat{u} + (\iota M - H_\rho^{-1})\hat{w} = 0, \tag{B7}$$

where c_s is background sound speed, $(\hat{u}, \hat{v}, \hat{w})$ is the peak velocity amplitude, $\hat{r} = \hat{\rho}/\overline{\rho}$ is the relative density amplitude, and $\hat{\Phi} = \hat{p}/\overline{\rho}$, in which $\hat{p}$ is the pressure amplitude. The full nonhydrostatic dispersion relation for gravity waves [e.g., (23-7) of Gossard and Hooke (1975)] follows from the equation set (B3)–(B7); that is,

$$m^2 = k^2\left(\frac{N^2 - \omega^2}{\omega^2 - f^2}\right) - \frac{1}{4H_\rho^2} + \frac{\omega^2}{c_s^2}. \tag{B8}$$

Polarization relations follow from (B3)–(B7). Eliminating $\hat{\Phi}$ between (B5) and (B6) and noting that $\hat{w} = -\iota\omega\hat{\zeta}$, then

$$\hat{r} = \frac{\hat{\rho}}{\overline{\rho}} = \left(\frac{N^2}{g}\right)[1 + a(m, \omega) + \iota b(m, \omega)]\hat{\zeta}, \tag{B9}$$

$$a(m, \omega) = (1 - \omega^2/N^2)\left(\frac{g}{c_s^2}\right)\left[\frac{-\Gamma}{m^2 + \Gamma^2}\right], \tag{B10}$$

$$b(m, \omega) = (1 - \omega^2/N^2)\left(\frac{g}{c_s^2}\right)\left[\frac{m}{m^2 + \Gamma^2}\right], \tag{B11}$$

where $\Gamma = -1/(2H_\rho) + g/c_s^2$ is the anisothermal form of Eckart's coefficient. Since $c_s^2 = \gamma gH$, then eliminating $\hat{r}$ between (B5) and (B6) yields

$$\hat{\Phi} = N^2\gamma H[a(m, \omega) + \iota b(m, \omega)]\hat{\zeta}, \tag{B12}$$

where γ is the ratio of specific heats. This replicates (23-6) of Gossard and Hooke (1975) and can be reexpressed in terms of the relative pressure perturbation

$$\frac{\hat{p}}{\overline{p}} = \frac{\hat{\Phi}}{R\overline{T}} = \left(\frac{N^2}{g}\right)\gamma[a(m, \omega) + \iota b(m, \omega)]\hat{\zeta}. \tag{B13}$$

A linearized perturbation expansion of the ideal gas law yields

$$\frac{\hat{T}}{\overline{T}} = \frac{\hat{p}}{\overline{p}} - \frac{\hat{\rho}}{\overline{\rho}}, \tag{B14}$$

which, on inserting (B9) and (B13), yields

$$\frac{\hat{T}}{\overline{T}} = \left(\frac{-N^2}{g}\right)\{1 - (\gamma - 1)[a(m, \omega) + \iota b(m, \omega)]\}\hat{\zeta}. \tag{B15}$$

Equations (B3)–(B7) also yield the polarization relation

$$\hat{w} = \frac{-(\omega^2 - f^2)}{k(N^2 - \omega^2)}(m + \iota\Gamma)\hat{u}. \tag{B16}$$

For an isothermal ($H = H_\rho$) nonrotating ($f = 0$) atmosphere, it can be shown that the dispersion and polarization relations (B8)–(B16) are the same as Eqs. (21)–(24) and (26) of Hines (1960).

On linearizing the tracer continuity equation (1b), assuming a height-varying mean tracer profile $\overline{n}(z)$, and substituting the wave solution (B1), we obtain

$$-\iota\omega\hat{n} + \frac{\partial\overline{n}}{\partial z}\hat{w} + \overline{n}\nabla\cdot\hat{\mathbf{U}} = 0. \tag{B17}$$

From (B16), it follows that

$$\nabla\cdot\hat{\mathbf{U}} = \iota k\hat{u} + \iota M\hat{w}, \tag{B18}$$

$$= \left\{\frac{1}{\gamma H} - \frac{N^2}{g}[a(m, \omega) + \iota b(m, \omega)]\right\}\hat{w}, \tag{B19}$$

whereupon (B17) yields

$$\frac{\hat{n}}{\overline{n}} = -\left\{\frac{1}{\gamma H} + \frac{1}{\overline{n}}\frac{\partial\overline{n}}{\partial z} - \frac{N^2}{g}[a(m, \omega) + \iota b(m, \omega)]\right\}\hat{\zeta}. \tag{B20}$$

Thus, on comparing (B9), (B13), (B15), and (B19) with the simplified parcel-based derivations in appendix A (see also sections 2 and 3), we see that the normalized terms $|a(m, \omega)|$ and $|b(m, \omega)|$ must be $\ll 1$ for the two sets of equations to be equal to a good approximation. We note from (B10) and (B11) that the frequency dependence of $a(m, \omega)$ and $b(m, \omega)$ is weak, so for simplicity we consider the limiting maximum values

$$a_{\max}(m) = \frac{g}{c_s^2}\left(\frac{-\Gamma}{m^2 + \Gamma^2}\right), \tag{B21}$$

$$b_{\max}(m) = \frac{g}{c_s^2}\left(\frac{m}{m^2 + \Gamma^2}\right) \tag{B22}$$

that arise for $(\omega/N)^2 \to 0$.

Since these maximum values depend only on the vertical wavenumber m, Fig. B1a plots $a_{\max}(m)$ and $b_{\max}(m)$ versus $\lambda_z = 2\pi/|m|$ for an isothermal atmosphere of $\overline{T} = 230$ K. Figures B1b and B1c show the corresponding maximum difference in magnitude and phase between the polarization relations (B9) and (B15) and the corresponding parcel approximations $\hat{\rho}/\overline{\rho} = -\hat{T}/\overline{T} = (N^2/g)\hat{\zeta}$ given by (18). Other plots (not shown) revealed that these differences increase (decrease) with decreasing (increasing) $\overline{T}$, and that the equality in magnitude of the density and temperature departures in Fig. B1b occurs only when the atmosphere is isothermal. For vertical wavelengths $\lambda_z \lesssim 20$ km, we see from Fig. B1 that the approximate parcel-based formulas of appendix A, approximated by the wave polarization relations (14) and (18), produce only small deviations in amplitude and phase from the full acoustic–gravity wave polarizations relations (B9) and (B15).

APPENDIX C

Photochemical Reponse of Ozone Mixing Ratio in a Vertically Displaced Air Parcel

We start with the parcel-based ozone rate equation (Lindzen and Goody 1965)

$$\frac{dq_{O_3}}{dt} = 2J_{O_2}q_{O_2} - \frac{2\epsilon k_{O_3}J_{O_3}q_{O_3}^2}{k_{O_2}n_{O_2}}. \tag{C1}$$

where

$$\frac{\epsilon k_{O_3}}{k_{O_2}} \approx \epsilon(1.3 \times 10^{28}\ \mathrm{m}^{-3})\left(\frac{T}{300\ \mathrm{K}}\right)^{2.3} \times \exp[-(2060\ \mathrm{K})/T] = G(T) \tag{C2}$$

(Demore et al. 1994). Equation (C1) differs from (2) and (31) only through insertion of an extra factor, ϵ, that scales the ozone destruction rate due to recombination with monatomic oxygen, k_{13}, to a net rate that resembles the one obtained when reactions with NO_x, HO_x, and ClO_x species are included (Zhu and Holton 1986).

We use (C1) and (C2) to describe the time evolution of ozone in a parcel displaced adiabatically by a small vertical distance ζ'. Since (A18a) holds for $n_{O_2}(z_2)/\overline{n}_{O_2}(z_2) - 1$, then

$$\frac{dq_{O_3}(z_2)}{dt} = 2J_{O_2}q_{O_2}(z_2) - \frac{2J_{O_3}}{\overline{n}_{O_2}(z_2)}G(T(z_2))q_{O_3}^2(z_2)\exp(-\zeta'/H_D), \tag{C3}$$

where $q_{O_3}(z_2) = \overline{q}_{O_3}(z_2) + q'_{O_3}(z_2)$ from (A19). We simplify (C3) by first noting that the background production/loss rate

$$\overline{R}_{O_3}(z_2) = 2J_{O_2}\overline{q}_{O_2}(z_2) - 2J_{O_3}\frac{G(\overline{T}(z_2))\overline{q}_{O_3}^2(z_2)}{\overline{n}_{O_2}} \approx 0. \tag{C4}$$

We then use a TMS expansion of $\exp(-\zeta'/H_D)$ and a truncated Taylor series expansion

$$G(\overline{T} + T') = G(\overline{T}) + T'\left(\frac{dG}{dT}\right)_{\overline{T}} = \overline{G} + G', \tag{C5}$$

where $T'(z_2) = T(z_2) - \overline{T}(z_2)$. Finally, on assuming constant q_{O_2} (no diffusive separation), constant J_x, and retaining only linear terms in the perturbation expansion of variables in (C3), we obtain, with the aid of (A13), (C4), and (C5),

$$\frac{dq_{O_3}(z_2)}{dt} = -\overline{B}(z_2)q'_{O_3}(z_2) - \overline{C}(z_2)T'(z_2), \quad \text{(C6)}$$

where

$$\overline{B}(z_2) = \frac{4J_{O_3}\overline{q}(z_2)G(\overline{T}(z_2))}{\overline{n}_{O_2}(z_2)}, \quad \text{(C7a)}$$

$$\overline{C}(z_2) = \frac{\overline{B}(z_2)\overline{q}(z_2)}{2\overline{T}^2(z_2)}\left[\overline{T}(z_2) - \left(\frac{d(\ln G)}{d(1/T)}\right)_{\overline{T}(z_2)}\right]. \quad \text{(C7b)}$$

Equation (C6) then yields the well-known ozone perturbation result of Lindzen and Goody (1965) (see section 3f), with the expressions (C7a) and (C7b) essentially the same as those derived by Zhu and Holton (1986).[1] More complete expressions for R_{O_3} with the NO_x, HO_x, and ClO_x rate terms included explicitly also leads to a linearized ozone deviation equation of the same form as (C6), although the formulas for the coefficients $\overline{B}$ and $\overline{C}$ are more complicated in this case (see, e.g., Stolarski and Douglass 1985).

REFERENCES

Alexander, M. J., and L. Pfister, 1995: Gravity wave momentum flux in the lower stratosphere over convection. *Geophys. Res. Lett.*, **22,** 2029–2032.

Bacmeister, J. T., S. D. Eckermann, L. Sparling, K. R. Chan, M. Loewenstein, and M. H. Proffitt, 1997: Analysis of intermittency in aircraft measurements of velocity, temperature and atmospheric tracers using wavelet transforms. *Gravity Wave Processes: Their Parameterization in Global Climate Models*, K. Hamilton, Ed., NATO ASI Series, Vol. I 50, Springer-Verlag, 85–102.

Bian, X., C. M. Berkowitz, and S. Zhong, 1996: Aircraft observations of the effects of internal gravity waves on ozone over the western North Atlantic. *J. Geophys. Res.*, **101,** 26 017–26 021.

Bird, J. C., S. R. Pal, A. I. Carswell, D. P. Donovan, G. L. Manney, J. M. Harris, and O. Uchino, 1997: Observations of ozone structures in the Arctic polar vortex. *J. Geophys. Res.*, **102,** 10 785–10 800.

Brasseur, G., and S. Solomon, 1984: *Aeronomy of the Middle Atmosphere*. 2d ed. Reidel, 452 pp.

Carslaw, K. S., M. Wirth, A. Tsias, B. B. Lou, A. Dörnbrack, M. Leutbecher, H. Volkert, M. Renger, J. T. Bacmeister, E. Reimer, and T. Peter, 1998: Increased stratospheric ozone depletion due to mountain-induced atmospheric waves. *Nature*, **391,** 675–678.

Chiu, Y. T., and B. K. Ching, 1978: The response of atmospheric and lower ionospheric layer structures to gravity waves. *Geophys. Res. Lett.*, **5,** 539–542.

Clemesha, B. R., V. W. J. H. Kirchoff, D. M. Simonich, H. Takahashi, and P. P. Batista, 1980: Spaced lidar and nightglow observations of an atmospheric sodium enhancement. *J. Geophys. Res.*, **85,** 3480–3489.

Collins, R. L., X. Tao, and C. S. Gardner, 1996: Gravity wave activity in the upper mesosphere over Urbana, Illinois: Lidar observations and analysis of gravity wave propagation models. *J. Atmos. Terr. Phys.*, **58,** 1905–1926.

Cox, R. M., J. M. C. Plane, and J. S. A. Green, 1993: A modelling investigation of sudden sodium layers. *Geophys. Res. Lett.*, **20,** 2841–2844.

Danielsen, E. F., R. S. Hipskind, W. L. Starr, J. F. Vedder, S. E. Gaines, D. Kley, and K. K. Kelly, 1991: Irreversible transport in the stratosphere by internal waves of short vertical wavelength. *J. Geophys Res.*, **96,** 17 433–17 452.

DeMore, W. B., S. P. Saunders, D. M. Golden, R. F. Hampson, M. J. Kurylo, C. J. Howard, A. R. Ravishankara, C. E. Kolb, and M. J. Molina, 1994: Chemical kinetics and photochemical data for use in stratospheric modeling. JPL Publ. 94-26, Jet Propulsion Laboratory, California Institute of Technology, Pasadena, CA, 273 pp. [Available from Jet Propulsion Laboratory, California Institute of Technology, Library Section, MS 111-120, 4800 Oak Grove Drive, Pasadena, CA 91109.]

Dudis, J. J., and C. A. Reber, 1976: Composition effects in thermospheric gravity waves. *Geophys. Res. Lett.*, **3,** 727–730.

Engelen, R. J., 1996: The effect of planetary waves on the total ozone zonal deviations in the presence of a persistent blocking anticyclone system. *J. Geophys. Res.*, **101,** 28 775–28 784.

Fritts, D. C., and P. K. Rastogi, 1985: Convective and dynamical instabilities due to gravity wave motions in the lower and middle atmosphere. *Radio Sci.*, **20,** 1247–1277.

——, J. R. Isler, G. E. Thomas, and Ø. Andreassen, 1993: Wave breaking signatures in noctilucent clouds. *Geophys. Res. Lett.*, **20,** 2039–2042.

——, ——, J. H. Hecht, R. L. Walterscheid, and Ø. Andreassen, 1997: Wave breaking signatures in sodium densities and OH nightglow, 2. Simulation of wave and instability structures. *J. Geophys. Res.*, **102,** 6669–6684.

Gardner, C. S., and J. D. Shelton, 1985: Density response of neutral atmospheric layers to gravity wave perturbations. *J. Geophys. Res.*, **90,** 1745–1754.

——, and D. G. Voelz, 1985: Lidar measurements of gravity wave saturation effects in the sodium layer. *Geophys. Res. Lett.*, **12,** 765–768.

Gibson-Wilde, D. E., R. A. Vincent, C. Souprayen, S. Godin, A. Hertzog, and S. D. Eckermann, 1997: Dual lidar observations of mesoscale fluctuations of ozone and horizontal winds. *Geophys. Res. Lett.*, **24,** 1627–1630.

Gossard, E. E., and W. H. Hooke, 1975: *Waves in the Atmosphere*. Elsevier, 456 pp.

Hansen, G., and U.-P. Hoppe, 1997: Lidar observations of polar stratospheric clouds and stratospheric temperature in winter 1995/96 over northern Norway. *Geophys. Res. Lett.*, **24,** 131–134.

Hedin, A. E., and H. G. Mayr, 1987: Characteristics of wavelike fluctuations in Dynamics Explorer neutral composition data. *J. Geophys. Res.*, **92,** 11 159–11 172.

Hess, P., 1990: Variance in trace constituents following the final stratospheric warming. *J. Geophys. Res.*, **95,** 13 765–13 779.

Hickey, M. P., and J. M. C. Plane, 1995: A chemical-dynamical model of wave-driven sodium fluctuations. *Geophys. Res. Lett.*, **22,** 2861–2864.

Hines, C. O., 1960: Internal gravity waves at ionospheric heights. *Can. J. Phys.*, **38,** 1441–1481; Corrigendum, **42,** 1425–1427.

Hoegy, W. R., L. H. Brace, W. T. Kasprzak, and C. T. Russell, 1990: Small-scale plasma, magnetic and neutral density fluctuations in the nightside Venus ionosphere. *J. Geophys. Res.*, **95,** 4085–4102.

Iribarne, J. V., and W. L. Godson, 1981: *Atmospheric Thermodynamics*. 2d ed. D. Reidel, 259 pp.

Jensen, E. J., and G. E. Thomas, 1994: Numerical simulations of the effects of gravity waves on noctilucent clouds. *J. Geophys. Res.*, **99,** 3421–3430.

Kao, C.-Y. J., S. Barr, A. Quintanar, D. Langley, G. A. Glatzmaier, and R. C. Malone, 1995: Numerical modeling of tracer transport within and out of the lower tropospheric Arctic region. *Geophys. Res. Lett.*, **22,** 941–944.

Kwon, K. H., D. C. Senft, and C. S. Gardner, 1988: Lidar observations of sporadic sodium layers at Mauna Kea Observatory, Hawaii. *J. Geophys Res.*, **93,** 14 199–14 208.

Lamb, K. G., and J. A. Shore, 1992: The influence of horizontal inhomogeneities on the propagation of high frequency linear

[1] Note that their Eq. 22 is wrong [cf. with (18)], which leads to a small error in their expression for $\overline{C}$.

internal gravity waves across a baroclinic flow. *J. Phys. Oceanogr.,* **22,** 965–975.

Langford, A. O., M. H. Proffitt, T. E. VanZandt, and J.-F. Lamarque, 1996: Modulation of tropospheric ozone by a propagating gravity wave. *J. Geophys. Res.,* **101,** 26 605–26 613.

Limpasuvan, V., and C. B. Leovy, 1995: Observation of the two day wave near the southern summer stratopause. *Geophys. Res. Lett.,* **22,** 2385–2388.

Lindzen, R. S., 1981: Turbulence and stress owing to gravity wave and tidal breakdown. *J. Geophys. Res.,* **86,** 9707–9714.

——, and R. Goody, 1965: Radiative and photochemical processes in mesospheric dynamics. Part I: Models for radiative and photochemical processes. *J. Atmos. Sci.,* **22,** 341–348.

Lutman, E. R., J. A. Pyle, M. P. Chipperfield, D. J. Lary, J. Kilbane-Dawe, J. W. Waters, and N. Larsen, 1997: Three-dimensional studies of the 1991/1992 Northern Hemisphere winter using domain-filling trajectories with chemistry. *J. Geophys. Res.,* **102,** 1479–1488.

Nagasawa, C., and M. Abo, 1995: Lidar observations of a lot of sporadic sodium layers in mid-latitude. *Geophys. Res. Lett.,* **22,** 263–266.

Newell, R. E., Z.-X. Wu, Y. Zhu, W. Hu, E. V. Browell, G. L. Gregory, G. W. Sachse, J. E. Collins Jr., K. K. Kelly, and S. C. Liu, 1996: Vertical fine-scale atmospheric structure measured from NASA DC-8 during PEM-West A. *J. Geophys. Res.,* **101,** 1943–1960.

Newman, P. A., and W. J. Randel, 1988: Coherent ozone-dynamical changes during southern hemisphere spring. *J. Geophys. Res.,* **93,** 12 585–12 606.

——, and M. R. Schoeberl, 1995: A reinterpretation of the data from the NASA Stratosphere-Troposphere Exchange Project. *Geophys. Res. Lett.,* **22,** 2501–2504.

Orsolini, Y. J., G. Hansen, U.-P. Hoppe, G. L. Manney, and K. H. Fricke, 1997: Dynamical modelling of wintertime lidar observations in the Arctic: Ozone laminae, and ozone depletion. *Quart. J. Roy. Meteor. Soc.,* **123,** 785–800.

Pierce, R. B., T. D. Fairlie, W. L. Grose, R. Swinbank, and A. O'Neill, 1994: Mixing processes in the polar night jet. *J. Atmos. Sci.,* **51,** 2957–2972.

Prata, A. J., 1990: Travelling waves in Nimbus-7 SBUV ozone measurements: Observations and theory. *Quart. J. Roy. Meteor. Soc.,* **116,** 1091–1122.

Randel, W. J., 1990: Kelvin wave-induced trace constituent oscillations in the equatorial stratosphere. *J. Geophys. Res.,* **95,** 18 641–18 652.

——, 1993: Global normal mode Rossby waves observed in stratospheric ozone data. *J. Atmos. Sci.,* **50,** 406–420.

——, and J. C. Gille, 1991: Kelvin wave variability in the upper stratosphere observed in SBUV data. *J. Atmos. Sci.,* **48,** 2336–2349.

Reber, C. A., A. E. Hedin, D. T. Pelz, W. E. Potter, and L. H. Brace, 1975: Phase and amplitude relationships of wave structure observed in the lower thermosphere. *J. Geophys. Res.,* **80,** 4576–4580.

Reid, S. J., and G. Vaughan, 1991: Lamination in ozone profiles in the lower stratosphere. *Quart. J. Roy. Meteor. Soc.,* **117,** 825–844.

Rind, D., and J. Lerner, 1996: Use of on-line tracers as a diagnostic tool in general circulation model development, 1, Horizontal and vertical transport in the troposphere. *J. Geophys. Res.,* **101,** 12 667–12 683.

Roble, R. G., and G. G. Shepherd, 1997: An analysis of wind-imaging interferometer observations of $O(^1S)$ equatorial emission rates using the thermosphere-ionosphere-mesosphere-electrodynamics general circulation model. *J. Geophys. Res.,* **102,** 2467–2474.

Rüster, R., P. Czechowsky, P. Hoffman, and W. Singer, 1996: Gravity wave signatures at mesopause heights. *Ann. Geophys.,* **14,** 1186–1191.

Salby, M. L., P. Callaghan, S. Solomon, and R. R. Garcia, 1990: Chemical fluctuations associated with vertically propagating equatorial Kelvin waves. *J. Geophys. Res.,* **95,** 20 491–20 505.

Senft, D. C., and C. S. Gardner, 1991: Seasonal variability of gravity wave activity and spectra in the mesopause region at Urbana. *J. Geophys. Res.,* **96,** 17 229–17 264.

Shibata, T., T. Itabe, K. Mizutani, and K. Asai, 1994: Pinatubo volcanic aerosols observed by lidar over Wakkanai, Japan. *Geophys. Res. Lett.,* **21,** 197–200.

Stanford, J. L., and J. R. Ziemke, 1993: Rossby-gravity waves in tropical total ozone. *Geophys. Res. Lett.,* **20,** 2239–2242.

Stolarski, R. S., and A. R. Douglass, 1985: Parameterization of the photochemistry of stratospheric ozone including catalytic loss processes. *J. Geophys. Res.,* **90,** 10 709–10 718.

Sugiyama, T., 1988: Response of electrons to a gravity wave in the upper mesosphere. *J. Geophys. Res.,* **93,** 11 083–11 091.

Teitelbaum, H., M. Moustaoui, J. Ovarlez, and H. Kelder, 1996: The role of atmospheric waves in the laminated structure of ozone profiles at high latitudes. *Tellus,* **48A,** 422–455.

Turner, J. S., 1973: *Buoyancy Effects in Fluids.* Cambridge University Press, 367 pp.

Wallace, J. M., and P. V. Hobbs, 1977: *Atmospheric Science: An Introductory Survey.* Academic Press, 467 pp.

Waugh, D. W., R. A. Plumb, R. J. Atkinson, M. R. Schoeberl, L. R. Lait, P. A. Newman, M. Loewenstein, D. W. Toohey, L. M. Avallone, C. R. Webster, and R. D. May, 1994: Transport out of the lower stratospheric Arctic vortex by Rossby wave breaking. *J. Geophys. Res.,* **99,** 1071–1088.

Weinstock, J., 1978: Theory of the interaction of gravity waves with O_2 $(^1\Sigma)$ airglow. *J. Geophys. Res.,* **83,** 5175–5185.

Wilson, J. C., W. T. Lai, and S. D. Smith, 1991: Measurements of condensation nuclei above the jet stream: Evidence for cross jet transport by waves and new particle formation at high altitudes. *J. Geophys. Res.,* **96,** 17 415–17 423.

Wirth, V., 1993: Quasi-stationary planetary waves in total ozone and their correlations with lower stratospheric temperature. *J. Geophys. Res.,* **98,** 8873–8882.

Zhu, X., and J. R. Holton, 1986: Photochemical damping of inertio–gravity waves. *J. Atmos. Sci.,* **43,** 2578–2584.

Ziemke, J. R., and J. L. Stanford, 1994: Quasi-biennial oscillation and tropical waves in total ozone. *J. Geophys. Res.,* **99,** 23 041–23 056.